Feshbach–Fano approach for calculation of Auger decay rates using equation-of-motion coupled-cluster wave functions. II. Numerical examples and benchmarks

Cite as: J. Chem. Phys. **154**, 084125 (2021); https://doi.org/10.1063/5.0036977 Submitted: 09 November 2020 . Accepted: 31 January 2021 . Published Online: 26 February 2021









ARTICLES YOU MAY BE INTERESTED IN

Feshbach-Fano approach for calculation of Auger decay rates using equation-of-motion coupled-cluster wave functions. I. Theory and implementation

The Journal of Chemical Physics 154, 084124 (2021); https://doi.org/10.1063/5.0036976

A Fock-operator complete active space self-consistent field (CAS-SCF) method combined with frozen-density embedding

The Journal of Chemical Physics 154, 084120 (2021); https://doi.org/10.1063/5.0037088

Energy natural orbitals

The Journal of Chemical Physics 154, 094103 (2021); https://doi.org/10.1063/5.0034810





Feshbach-Fano approach for calculation of Auger decay rates using equation-of-motion coupled-cluster wave functions. II. Numerical examples and benchmarks

Cite as: J. Chem. Phys. 154, 084125 (2021); doi: 10.1063/5.0036977 Submitted: 9 November 2020 • Accepted: 31 January 2021 • Published Online: 26 February 2021







Wojciech Skomorowski^{a)} D and Anna I. Krylov^{a)}





AFFILIATIONS

Department of Chemistry, University of Southern California, Los Angeles, California 90089, USA

a) Authors to whom correspondence should be addressed: skomorow@usc.edu and krylov@usc.edu

ABSTRACT

X-ray photon absorption leads to the creation of highly excited species, which often decay through the Auger process. The theoretical treatment of Auger decay is challenging because of the resonance nature of the initial core-excited or core-ionized states and the continuous nature of the ejected electron. In Paper I [W. Skomorowski and A. I. Krylov, J. Chem. Phys. 154, 084124 (2021)], we have introduced a theoretical framework for computing Auger rates based on the Feshbach-Fano approach and the equation-of-motion coupled-cluster ansätze augmented with core-valence separation. The outgoing Auger electron is described with a continuum orbital. We considered two approximate descriptions—a plane wave and a Coulomb wave with an effective charge. Here, we use the developed methodology to calculate Auger transition rates in core-ionized and core-excited benchmark systems (Ne, H2O, CH4, and CO2). Comparison with the available experimental spectra shows that the proposed computational scheme provides reliable ab initio predictions of the Auger spectra. The reliability, cost efficiency, and robust computational setup of this methodology offer advantages in applications to a large variety of systems.

Published under license by AIP Publishing. https://doi.org/10.1063/5.0036977

I. INTRODUCTION

By providing tunable high-energy radiation, advanced light sources enable a variety of x-ray based spectroscopies. 1-3 Recent advances in beam quality greatly expanded the possible applications of x rays, giving rise to a proliferation of techniques, including those operating in time-resolved and non-linear regimes.¹⁻ Fundamentally, these spectroscopies exploit electronic transitions involving core orbitals, whose localized nature enables the local environment to be probed, thus providing complementary information to valence-based techniques.

As in the case of vacuum ultraviolet (VUV)-based techniques,6 theoretical modeling is required to relate experimental measurements to molecular structures. Consequently, experimental advances have stimulated the development of theoretical techniques for core-level transitions. Owing to their special properties, accurate description of core-level states is much more challenging than the description of valence states.⁵ Despite significant progress in extending quantum chemistry to core-level states, theoretical tools for modeling x-ray spectroscopies are still lagging behind experimental capabilities, creating a bottleneck for maximizing the scientific impact of advanced light-source facilities.

Recently, many quantum chemistry methods have been adapted to treat core-level states by utilizing the core-valence separation (CVS) scheme, which decouples highly excited core-level states from the continuum of valence excitations and allows one to describe metastable core-level states by \mathcal{L}^2 -integrable wave functions. By using CVS, many-body methods developed for bound ionized and excited states have been adapted to treat highly energetic unbound (with respect to electron ejection) core-level states. In particular, equation-of-motion coupled-cluster (EOM-CC) methods⁸⁻¹¹ have been extended to model core ionization and core excitation processes, including non-linear regimes. 12-22 The benchmarks and applications illustrated the excellent performance of CVS-enabled EOM-CC methods. 14,21,23-26 Moreover, Park et al. 27 have recently presented a time-dependent EOM-CC formulation, which enables calculations of the core spectra without invoking CVS. This work has also shown that by systematic improvement in correlation treatment, one-electron basis sets, orbital relaxation, and relativistic effects, the EOM-CC based protocol ultimately delivers a sub-eV accuracy in core-excitation energies. Importantly, in all these extensions, the continuum was simply ignored. Consequently, such calculations are only able to deliver the energies of the core-level states and intensities of the spectral transitions. The lifetimes of the core-level states and the respective broadening of the spectral lines could not be computed. In Paper I, 28 we presented the extension of the theory to compute the decay rates of the core-level states.

The core-level states are Feshbach resonances that can decay by a two-electron process, called Auger decay, and its nonlocal variants—intermolecular Coulomb decay and electron-transfer mediated decay. As illustrated in Fig. 1, Auger decay is a process in which an N-electron highly excited core-level state decays into an N-1 electron valence state and a free electron. The theoretical framework, described in Paper I, 28 is based on the Feshbach-Fano treatment of resonance phenomena. In this approach, the full function space is artificially divided into the bound and unbound spaces, and the resonances are described in terms of the interacting diabatic-like states, representing the bound part of the resonance and the continuum decay channels, respectively. The essential feature of our formulation of the Feshbach-Fano treatment is the use of CVS to define the Feshbach projectors. We use EOM-CC to describe the bound part of the wave function in the initial and final states of the Auger decay and use continuum orbitals to represent the Auger electrons. The versatility of the EOM-CC ansätze facilitates efficient treatment of complex multi-configurational and open-shell wave functions, as well as systematic inclusion of electron correlation.

To describe the decay channels, we combine many-body electronic states described by equation-of-motion coupled-cluster singles and doubles (EOM-CCSD) with a continuum orbital. In this work, we approximate the continuum orbital by a plane wave or a Coulomb wave, which avoids numerical integration in the calculations of mixed bound-continuum electron-repulsion integrals. The working equations for the calculations of the partial autoionization widths are expressed in terms of one- and two-body Dyson functions, ^{29,30} contracted with the bound-continuum integrals.

In this paper, we illustrate the performance of the new methodology by calculating Auger decay rates in several well-characterized systems. Specifically, we considered the non-resonant Auger effect due to a single K-shell vacancy in the Ne atom and H_2O , CH_4 , and CO_2 (C-edge) molecules and resonant Auger effect in core-excited Ne $(1s \rightarrow 3p)$ and $CO_2(C1s \rightarrow \pi_u^*)$.

II. THEORETICAL PROTOCOL AND COMPUTATIONAL DETAILS

Within our approach, the calculations of Auger decay rates require two essential components: two-body Dyson functions and mixed bound-continuum two-electron integrals. The two-body Dyson functions are bound-domain properties, and they are calculated from appropriate EOM-CC solutions, as illustrated in Fig. 1. All systems in this study have closed-shell ground states, which served as reference states in the CCSD and EOM-CCSD calculations. Initial states for non-resonant Auger decay were obtained from the ionization potential (IP) variant of EOM-CCSD with core-valence separation (CVS-EOM-IP-CCSD, removal of one core electron), whereas the final states (decay channels) were computed

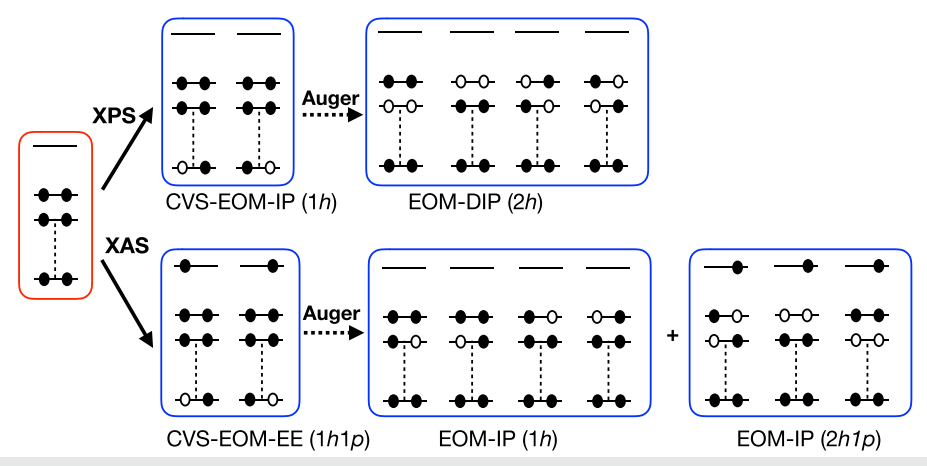


FIG. 1. Initial and target states corresponding to different types of the Auger effect. Top row illustrates regular Auger decay, which is relevant for x-ray photoionization spectroscopy (XPS). The initial and decay states can be described by CVS-EOM-IP and EOM-DIP, respectively. The bottom row illustrates resonant Auger decay, which is relevant to x-ray absorption spectroscopy (XAS). The initial state in resonant Auger decay can be described by CVS-EOM-EE. The decay states can be described by EOM-IP-CCSD. In resonant participator decay, the initially excited electron is ejected—hence, the decay states are described by 1h EOM-IP operators. In resonant spectator decay, the initially excited electron remains and another electron is ejected. leading to excited states of the ion that requires 2h1p EOM-IP operators.

by means of the double ionization potential (DIP) variant^{33–37} of EOM-CCSD (EOM-DIP-CCSD, removal of two valence electrons). This way of generating the final electronic states for the purpose of interpreting Auger spectra was originally suggested in Ref. 33, where it has also been shown that various EOM-CC variants can describe double ionization potentials with an accuracy better than an eV for small molecules.

For resonant Auger decay, the initial state was computed with the excitation energy (EE) variant^{9,38,39} of EOM-CCSD with corevalence separation (CVS-EOM-EE-CCSD, excitation of core electrons), whereas the corresponding final states were described with the IP variant of EOM-CCSD (EOM-IP-CCSD, removal of one valence electron). Core electrons were frozen in all valence calculations and treated in accordance with the frozen-core CVS prescription¹⁴ in the calculations of core-level states. The frozen core was defined as comprising K-shells on Ne/O/C atoms. Unless stated otherwise, in bound-state calculations, we employed a fully uncontracted 6-311+G(3df) basis set^{40,41} for all atoms. As has been recently shown,²³ this one-electron basis offers a good balance between cost and accuracy for core ionized/excited states. The calculations were carried out using MP2/aug-cc-pVTZ-optimized structures; the respective Cartesian coordinates are given in the supplementary material.

Here, we test two simple approaches for the continuum orbital: a plane wave and a Coulomb wave expanded in terms of an auxiliary basis set of the products of Gaussian and plane wave (GPW) functions. The details of the implementation of mixed GTO-GPW integrals are described in Paper I.28 As for the Coulomb wave, the expansion coefficients in terms of the GPW functions were generated following the pseudo-partial wave method of Szczygieł et al. 42 The parameters of the auxiliary GPW basis set for each energy and pseudo-partial wave were determined through the optimization by means of the differential evolution algorithm. For the optimization procedure, the reference values of the Coulomb wave were generated on a radial grid from 0 to 2 bohr with a spacing of 0.05 bohr and from 2 to 10 bohrs with a spacing of 0.1 bohr. Because Auger decay is a rather local phenomenon, with core orbitals primarily contributing to the effect, there is no need for a more-extended representation of the continuum orbital in the calculations of the two-electron integrals. Based on the numerical tests, we truncated the pseudo-partial wave expansion at $l_{max} = 6$, with each pseudopartial wave represented in terms of n = 10 Gaussian components. The choice of the effective charge for the Coulomb wave is discussed

All electronic structure calculations were carried out with the Q-Chem package. 43,44 The optimization of the GPW basis set for Coulomb wave expansion was performed with the Mathematica package.4

III. RESULTS AND DISCUSSION

A. Ne $(1s^{-1})$

The K-shell vacancy in the Ne atom has been, arguably, the most frequently studied example of the Auger effect, both experimentally and theoretically. $^{46,48-52}$ The Auger spectrum in Ne⁺(1s⁻¹) is particularly suitable for in-depth analysis as it features sharp

discrete lines with no vibrational broadening or vibronic coupling, with easily identified diagram (i.e., main, Koopmans-like) transitions and a satellite structure. Therefore, the $Ne^+(1s^{-1})$ state is often used as a test case to validate various theoretical approaches for Auger rates. In the Ne K-LL Auger spectrum, there are five main lines, corresponding to the formation of the residual Ne²⁺ ion in the following states: ${}^{1}D(2p^{-2})$, ${}^{1}S(2p^{-2})$, ${}^{3}P(2s^{-1}p^{-1})$, ${}^{1}P(2s^{-1}2p^{-1})$, and ${}^{1}S(2s^{-2})$. Branching ratios for populating those five channels have been reported a few times, with high consistency of the results. 46 This is in contrast to a significant uncertainty in the experimental determination of the total natural width of the $Ne^+(1s^{-1})$ level. The reported experimental natural linewidths vary from roughly 0.21 eV to 0.30 eV. 48,53-56 In the present work, we refer to the numbers reported in a recent high-precision spectroscopic study on Ne⁺ ions near the K-edge. ⁴⁸ Based on measured photo-ionization cross sections, the authors determined the total natural width of the $\text{Ne}^+(1s^{-1})$ level to be 261 ± 5 meV, which includes contribution from both radiative and Auger decay, and the latter can be further split into one, two, and three-electron emission channels. Here, we focus exclusively on one-electron Auger decay channels, for which partial width is estimated to be 242 ± 10 meV, based on relative photoionization cross sections and resonance strengths reported in Table 5/6 of Ref. 48.

Table I shows energies for the main Ne K-LL Auger channels, calculated with various one-electron basis sets and compared with the experimental values from Ref. 46. In accordance with the results of a recent benchmark study,²³ the relatively compact 6-311+G(3df) basis set (fully uncontracted) provides energies of the same quality as more-sizable Dunning-type bases. Our calculated energies differ from the experimental ones by 0.5 eV to $\sim 1.5 \text{ eV}$, which is within the error bars of the method. 14 The remaining error is due to the neglect of the relativistic contributions,²¹ higher-order correlation effects, and an incomplete one-electron basis set. The energies reported in Table I also neglect the resonance shift, a contribution that is relatively expensive to calculate. It is known that for Auger resonances, the energy shift Δ_n is a minor correction (usually <0.2 eV⁵⁷), and thus, it is well within the error of our main energy term E_n .

Tables II and III present absolute values and branching ratios for Ne K-LL Auger transition rates, obtained with different models for the continuum orbital and compared with the most accurate experimental results. The experimental values for partial widths reported in the last column of Table II are obtained from the analysis of the results from Refs. 46 and 48, where we have assumed the total one-electron Auger width of 242 ± 10 meV from Ref. 48 and the branching ratios from Ref. 46.

As noted above, we employed a simple model for the continuum orbital: either a plane wave or a Coulomb wave. A Coulomb wave requires a specification of an effective charge of the residual ion. Depending on the modeled properties, several protocols for estimating optimal effective charges have been proposed. We have tested three different models to generate optimal effective charges. The first and simplest model employs Slater rules,⁵⁸ which provide universal screening constants for each atomic shell. Based on the Slater rules, the residual ion Ne²⁺ induces an effective charge equal to 6.2. Slater rules do not account for differences between sub-shells, so they predict the same screening due to 2s and 2p electrons. This limitation has been removed in a couple of other studies aiming to determine optimal screening constants.4

TABLE I. Auger electron energies (in eV) corresponding to *K–LL* transitions in the core-ionized neon atom (calculated with the fc-CVS-EOM-CCSD method and various one-electron basis sets).

Channel	u-6-311+G(3df)	u-aug-cc-pVTZ	u-d aug-cc-pVTZ	Expt. ⁴⁶
1 D $(2p^{-2})$	803.62	803.74	803.74	804.30(8)
$^{1}S(2p^{-2})$	800.09	800.21	800.21	800.60(8)
$^{3}P(2s^{-1}2p^{-1})$	781.19	781.24	781.24	782.24(8)
$^{1}P(2s^{-1}2p^{-1})$	770.50	770.56	770.56	771.71(8)
$^{1}\text{S}(2s^{-2})$	746.55	746.54	746.54	748.14(8)

TABLE II. Partial and total Auger decay widths (in meV) for *K-LL* transitions in the core-ionized neon atom. Calculations used either a plane wave or Coulomb wave (with specified effective charges) to model the outgoing electron.

Channel	Plane wave $(Z_{eff} = 0)$	Slater $(Z_{eff} = 6.2)$	Updated Slater ^a	$Z_{eff} \sim \sqrt{1/\langle r^2 \rangle}^{\rm b}$	Expt. ^c
1 D $(2p^{-2})$	154.9	105.5	109.8	117.5	147 ± 6
$^{1}S(2p^{-2})$	4.4	12.2	12.2	10.5	23 ± 1
$^{3}P(2s^{-1}2p^{-1})$	116.5	19.2	15.0	23.8	15 ± 1
$^{1}P(2s^{-1}2p^{-1})$	4.8	41.5	43.0	39.2	42 ± 2
$^{1}\text{S}(2s^{-2})$	19.0	28.0	23.1	27.1	15 ± 1
Total	299.6	206.4	203.1	218.1	242 ± 10

^aBased on screening constants optimized for ionic configurations (OHAO model from Ref. 47): $Z_{eff} = 5.8/5.8/6.8/6.8/7.8$ for respective channels.

Here, we tested modified Slater rules and resulting effective charges based on the approach from Ref. 47, where the optimal screening constants were generated by fitting energies of multiple atomic and ionic states with the primary configuration of the type $1s^22s^m2p^n$. By explicitly including the ionic configurations in the fit, this model better reflects the physics we aim to describe—namely, the outgoing electron moving in the field of the Ne²⁺ ion. We refer to the effective charges, based on Ref. 47, as "updated Slater" in Tables II and III.

Following a different approach, one can obtain an effective charge based on the size of the valence orbital vacated in the Auger decay. To this end, one can employ the relation for the hydrogen-like ion,

$$\langle r^2 \rangle = \frac{n^2}{2Z_{eff}^2} \left[5n^2 + 1 - 3\langle l^2 \rangle \right],\tag{1}$$

which links the size of the orbital $\langle r^2 \rangle$ with its effective charge Z_{eff} , principle quantum number n, and angular momentum $\langle l^2 \rangle$. For an

TABLE III. Relative widths (given in %) for *K–LL* transitions in the core-ionized neon atom (calculations with the same models for the outgoing electron as in Table II).

Channel	Plane wave $(Z_{eff} = 0)$	Slater $(Z_{eff} = 6.2)$	Updated Slater ⁴⁷	$Z_{e\!f\!f} \sim \sqrt{1/\langle r^2 angle}$	Expt. ⁴⁶
1 D $(2p^{-2})$	51.7	51.1	54.1	53.9	60.9
$^{1}S(2p^{-2})$	1.5	5.9	6.0	4.8	9.5
$^{3}P(2s^{-1}2p^{-1})$	38.9	9.3	7.4	10.9	6.3
$^{1}P(2s^{-1}2p^{-1})$	1.6	20.1	21.2	18.0	17.2
$^{1}S(2s^{-2})^{1}$	6.3	13.6	11.4	12.4	6.1

^b Based on the size of the vacant valence orbitals: $Z_{eff} = 4.9/4.9/5.7/5.7/6.6$ for respective channels. For $2s^{-1}2p^{-1}$ configuration, the geometrical average is applied.

^cExperimental data^{46,48} derived from Refs. 46 and 48 (see the text for the explanations).

atom, all requisite quantities for computing $Z_{\rm eff}$ from this equation are easily obtainable. As expected, both the updated Slater rules and $\langle r^2 \rangle$ approach predict a larger screening due to 2s than 2p electrons and, consequently, a smaller effective charge for $2p^{-2}$ than for $2s^{-2}$ configurations of Ne²⁺. The exact values of the effective charges for all channels within each model are given in the footnote of Table II.

As shown in Tables II and III, a plane wave continuum orbital leads to rather poor results for the Auger partial widths and branching ratios, although the total width is reasonable and the channel with the largest intensity (¹D) is identified correctly. The results can be significantly improved when a Coulomb wave with an appropriate effective charge is employed to model the free electron. Indeed, all tested sets of the effective charges correct absolute and relative intensities for the ¹P and ³P channels, with ¹D remaining as the dominant channel. In contrast, the results for the two ¹S channels do not show much improvement with any of the tested Coulomb waves. To investigate this further, Fig. 2 shows how each partial width changes as a function of the Coulomb wave charge Z_{eff} . One can see that for 1 D, 1 P, and 3 P, one can pick Z_{eff} such that the calculated widths match the experimental values. Also, as expected, the optimal Z_{eff} for ¹D is smaller than those for ¹P and ³P channels. In contrast, there is no reasonable $Z_{\it eff}$ that would allow one to adjust theoretical widths for both ¹S channels. This is an illustration of the importance of the inter-channel coupling for the K-LL Auger decay in Ne. It was shown previously⁴⁹ that the two ¹S channels strongly mix with each other and the coupling leads to the redistribution of the Auger intensities between the two channels. Within the independent channel model, the present calculations cannot reproduce the effect

of the channel mixing. At the same time, the inter-channel coupling does not affect the sum of the two ¹S intensities, and this sum is reproduced accurately by all Coulomb wave models in Table II. As to the total Auger width, the last tested model, with effective charges based on the orbital size, gives the best number, which is still, however, ~20 meV off the experimental value. This discrepancy is mostly due to significantly underestimating the Auger rate for the ¹D channel, which can be traced back to the deficiency of the singlechannel calculations. As shown in Ref. 50, multi-channel approaches increase the ¹D rate by around 10% compared to the single-channel rate. Overall, the simple model for the continuum orbital based on a Coulomb wave and an appropriate effective charge is able to reproduce the main features and relative intensities of the Ne *K*–*LL* Auger spectrum fairly well, which validates our approach. To resolve the remaining discrepancies, it is necessary to include the interaction between the continuum channels, which is beyond the scope of the present study.

Before discussing the results for the other benchmark systems, let us address the convergence of the calculated widths with respect to the details of the computational protocol. The first question is the convergence with respect to the one-electron basis set used for the bound domain electronic structure calculations. The Auger widths for Ne *K-LL* obtained with three one-electron basis sets, shown in the supplementary material, are in very good agreement with each other. The convergence for the widths is as good as for the energies (see Table I). This is simply because within our approach, the one-electron basis set only affects the two-body Dyson functions (i.e., properties purely from the bound domain), whereas the continuum orbital is separated from the bound domain and it is described with a different function. Therefore, it is more important to address the

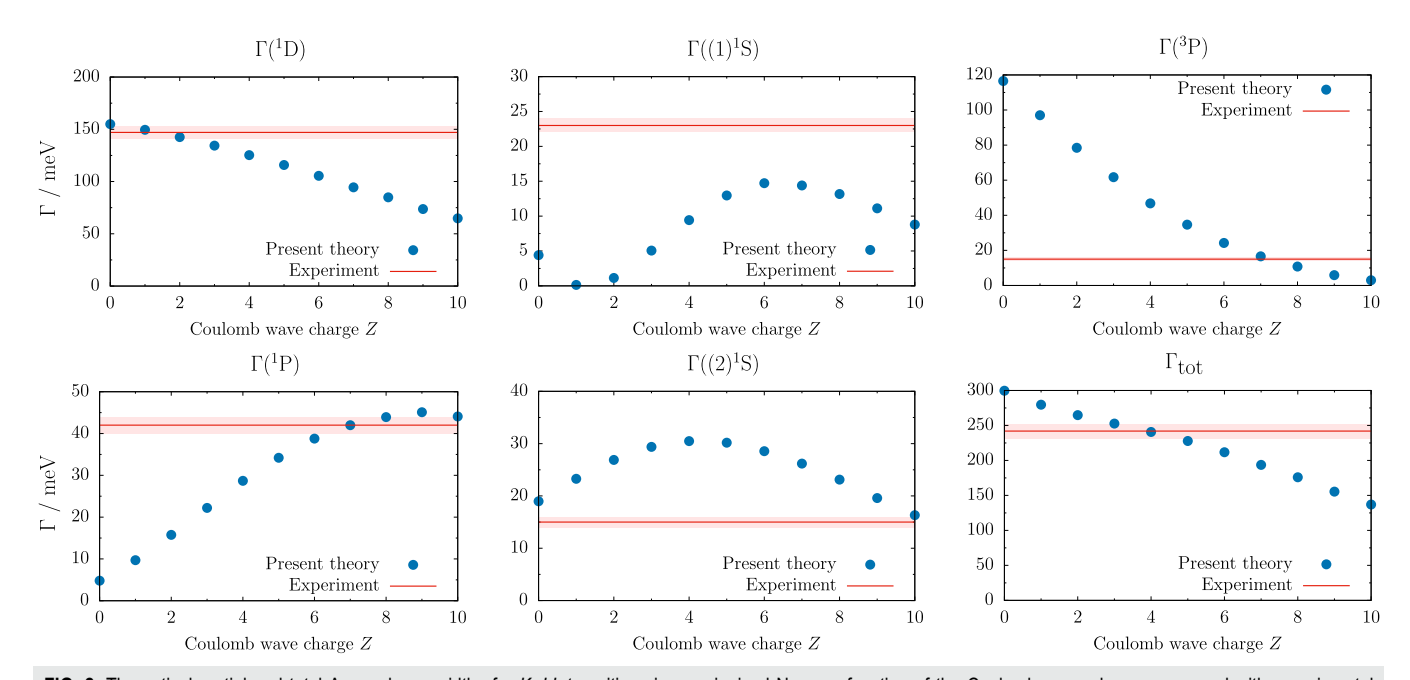


FIG. 2. Theoretical partial and total Auger decay widths for K–LL transitions in core-ionized Ne as a function of the Coulomb wave charge compared with experimental data^{46,48} (shown as the horizontal red line with shaded areas indicating error bars as given in Table II).

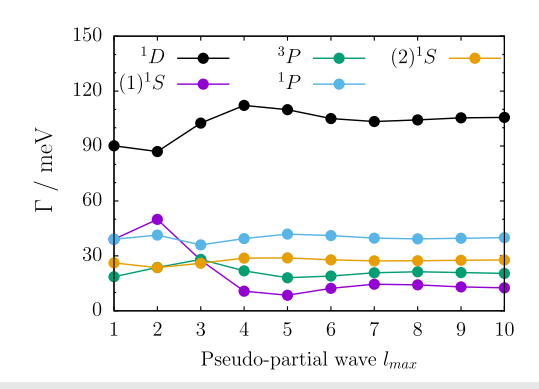


FIG. 3. Convergence of the partial decay widths for K–LL transitions in coreionized Ne with respect to pseudo-wave expansion of the Coulomb wave function. Calculations are performed with $Z_{\rm eff}$ = 6.2.

convergence with respect to the parameters used to model the continuum orbital. While the representation of a plane wave does not involve approximations, for a Coulomb wave, we employ the auxiliary basis set and the pseudo-partial wave expansion. Figure 3 shows how the partial widths converge with respect to the pseudo-partial waves (for $Z_{eff}=6.2$). For all channels, the convergence is rather fast, and already, for $l_{max}=6$, the results have essentially converged. This is encouraging, given that the scattering energies considered here are on the order of 800 eV and standard partial wave expansion would require many more terms.

B. $H_2O(1s^{-1})$

Similar to the Ne atom, the Auger electron spectrum due to a single K-shell vacancy in a water molecule has been the subject of extensive studies, both theoretical and experimental. 61-67 Numerous theoretical investigations have revealed the effects of nuclear dynamics, electronic correlation, and satellite transitions in the Auger profile of H₂O. 61,64,66 Decay of the single core vacancy in H₂O is of the *K*–*LL* type, and to a large extent, it is reminiscent of the corresponding K-LL decay in the isoelectronic Ne atom. However, the lower symmetry of H₂O results in a large number of distinct final channels with two vacancies in the valence shell. Additionally, Franck-Condon broadening leads to a broad spectral profile, in contrast to discrete lines observed in the Auger spectrum of atomic neon. A simple molecular orbital picture permits the division of the main Auger transitions in H₂O into three regions: (1) from ~500 eV to ~485 eV, where two electrons are removed from the outer-valence shell $(3a_11b_11b_2)$, (2) from ~480 eV to ~460 eV, where one electron is removed from the outer-valence shell and another one from the inner valence shell (2 a_1), and (3) from ~460 eV to ~450 eV, where two electron are removed from the inner-valence shell $(2a_1)$. As shown by the experimental Auger spectrum in the upper panel of Fig. 4, the largest intensity appears in the first region, at its high-energy end, similar to the Ne atom. 62

Table IV shows the results of our calculations for the main Auger transition channels in H_2O . We tested two models for the continuum orbital: a plane wave and a Coulomb wave with a uniform effective charge of 4.9 for all channels, which is derived from the Slater rules applied to an isolated oxygen atom. The computed

Auger spectra are shown in the two lower panels of Fig. 4; these profiles were obtained by convolution of the calculated intensities with a Gaussian function with a fixed full width at half maximum equal to 1.0 eV. Table IV also includes the transition rates computed by Inhester *et al.*, ⁶¹ which are the most accurate in terms of reproducing the experimental profile and can serve as the reference for individual partial widths.

The analysis of Table IV and Fig. 4 shows that our method is able to reproduce the main features of the spectrum; however, some of the channel rates are significantly over- or under-estimated. The model with the plane wave assigns much too high an intensity to triplet channels (depicted with green bars in Fig. 4) between 480 eV and 475 eV. This is rectified when the Coulomb wave is employed to represent the continuum orbital: according to Table IV, the rates for triplet channels obtained with the Coulomb wave agree well with the reference theoretical data. A shortcoming, which is not remedied by the Coulomb wave model, is the overestimation of the lowest 1A_1 channel and the underestimation of the highest 1A_1 and 1B_1 channels. As in the case of Ne, this problem can be traced back to the inter-channel coupling, neglected in our approach. Indeed,

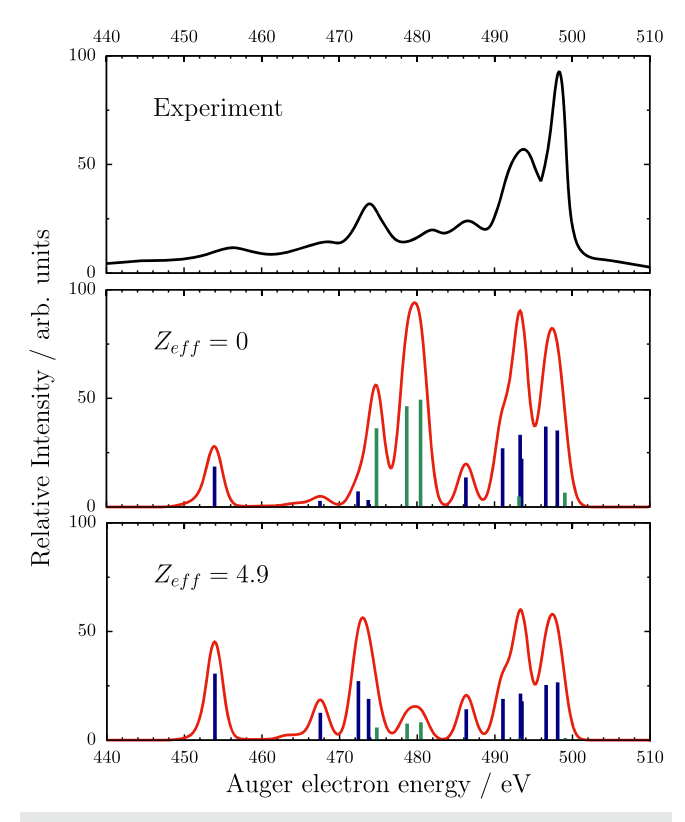


FIG. 4. Experimental⁶² and computed Auger spectra for the singly ionized water molecule. Middle and bottom panels show the calculations with a plane wave and a Coulomb wave, respectively. Theoretical curves obtained from the stick spectra by assuming a constant Gaussian broadening of 1.0 eV FWHM. Darkblue sticks correspond to singlet channels, while green sticks correspond to triplet channels

the $^1A_1(2a_1^{-2})$ channel with two inner vacancies corresponds to the $(2)^1S$ channel in Ne decay for which the rate was also significantly overestimated, whereas the two channels with the highest energy $[^1D$ and $(2)^1S]$ turned out to be underestimated. Our results, which significantly overestimated the lowest 1A_1 channel rate, are in line with the previous calculations based on the Stieltjes imaging or Dyson propagator methods. Calculations from Ref. 61 have also shown that it is necessary to include nuclear dynamics effects to obtain the correct shape of the peaks at the high-energy end and that a homogeneous broadening is not sufficient.

Using water as an example, we can illustrate the importance of electronic correlation and configuration mixing for the Auger widths. The magnitude of these effects for different channels can be estimated from the norms of the corresponding two-body Dyson functions. For the diagram transitions in H_2O , these norms vary between 1.92 and 1.55 (the complete data are given in Table S2 of the supplementary material), whereas for the uncorrelated Hartree–Fock/Koopmans states, the norms are exactly 2. These numbers show that configuration mixing and electronic correlation are important not only for the peak positions but also for the widths of the Auger peaks, i.e., the decay widths would be affected by at least 5%–25% due to the norms of the Dyson functions alone.

As to the total Auger decay width, our models yield 175.1 meV for a plane wave and 121.7 meV for a Coulomb wave with Z_{eff} = 4.9; these numbers should be compared with the experimentally determined natural linewidth of K-shell vacancy in H_2O of

TABLE IV. Energies (in eV), total (Γ_{tot}) and partial (Γ_i) widths (in meV) for the main channels in the Auger decay of *K*-shell ionized water. Calculations of the widths used either a plane wave or a Coulomb wave with effective charge Z_{eff} = 4.9 for all channels.

		Γ_i (meV)			
Channel	Energy (eV)	$Z_{eff} = 0$	$Z_{eff} = 4.9$	Theory from Ref. 61	
${}^{3}\mathrm{B}_{1}(3a_{1}^{-1}1b_{1}^{-1})$	499.07	3.3	0.5	0.4	
$^{1}A_{1}(1b_{1}^{-2})$	498.09	17.6	13.3	19.0	
$^{1}B_{1}(3a_{1}^{-1}1b_{1}^{-1})$	496.61	18.5	12.7	18.0	
$^{3}\text{A}_{2}(1b_{1}^{-1}1b_{2}^{-1})$	495.07	0.0	0.0	0.0	
$^{1}A_{1}(3a_{1}^{-2})$	493.49	11.1	8.9	13.1	
$^{1}\text{A}_{2}(1b_{1}^{-1}1b_{2}^{-1})$	493.31	16.6	10.7	15.2	
$^{3}\mathrm{B}_{2}(3a_{1}^{-1}1b_{2}^{-1})$	493.17	2.4	0.4	0.3	
${}^{1}\mathrm{B}_{2}(3a_{1}^{-1}1b_{2}^{-1})$	491.04	13.5	9.5	13.2	
$^{1}\text{A}_{1}(1b_{2}^{-2})$	486.32	6.8	7.1	9.8	
${}^{3}\mathrm{B}_{1}(2a_{1}^{-1}1b_{1}^{-1})$	480.47	24.7	4.1	3.0	
3 A ₁ $(2a_{1}^{-1}3a_{1}^{-1})$	478.69	23.2	3.8	2.6	
$^{3}\mathrm{B}_{2}(2a_{1}^{-1}1b_{2}^{-1})$	474.79	18.1	2.9	1.6	
$^{1}B_{1}(2a_{1}^{-1}1b_{1}^{-1})$	473.73	1.6	9.5	10.0	
1 A ₁ $(2a_{1}^{-1}3a_{1}^{-1})$	472.42	3.6	13.6	11.0	
$^{1}\text{B}_{2}(2a_{1}^{-1}1b_{2}^{-1})$	467.51	1.4	6.3	6.6	
$^{1}A_{1}(2a_{1}^{-2})$	453.93	9.3	15.3	4.1	
$\Gamma_{ m tot}$		175.1	121.7	145.6	

 160 ± 5 meV. ⁶⁹ Thus, as for Ne, the model with the plane wave overestimates the total width, whereas the Coulomb wave underestimates it. The underestimation is expected because our calculations only account for a single-electron Auger decay pathway, neglecting other possible pathways such as radiative decay or via coupling to the continua with two or more Auger electrons. Moreover, we do not perform full diagonalization of the EOM-CC Hamiltonian: the channels included in the total rate are those with Auger electron energies down to 450 eV, and any contribution from the lower energy range is neglected. Therefore, our model with the Coulomb wave provides a lower bound of the total lifetime.

C. CH₄ $(1s^{-1})$

In terms of symmetry, CH_4 is an intermediate case between the isoelectronic Ne atom and the H_2O molecule. Its ground-state configuration is $1a_1^22a_1^21t_2^6$, with degenerate t_2 orbitals. From this closed-shell configuration, one can derive seven main channels for the K–LL Auger decay, which is fewer than for H_2O (16) but more than for Ne (5). The Auger electron spectrum for CH_4 following single K-shell ionization has been measured a few times with different techniques, yielding very consistent shapes. The spectrum is simple and features three distinct peaks of decreasing intensity,

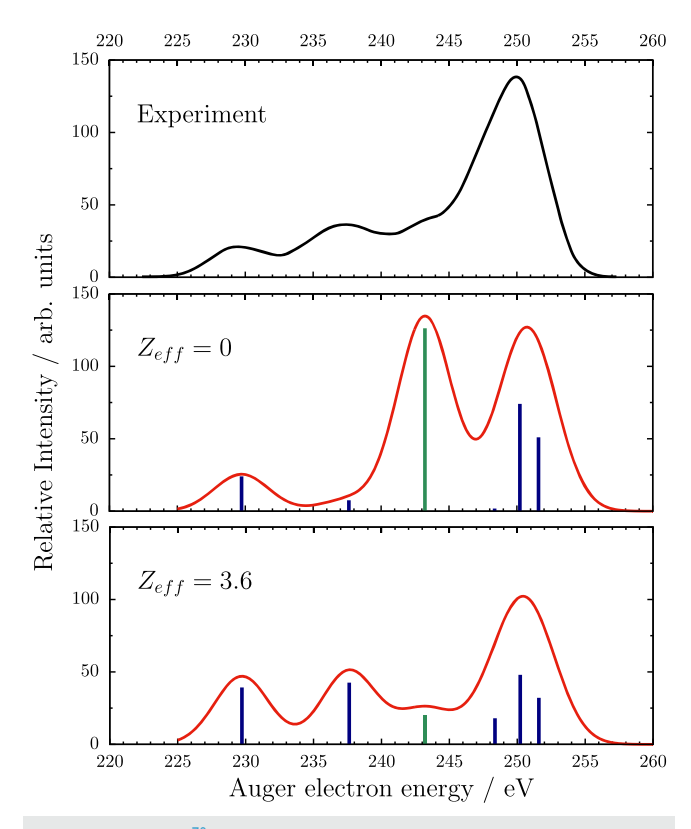


FIG. 5. Experimental⁷⁰ and computed Auger spectra for the singly ionized methane molecule. Middle and bottom panels show the calculations with a plane wave and a Coulomb wave, respectively. Theoretical curves obtained from the stick spectra by assuming a constant Gaussian broadening of 2.0 eV FWHM. Dark-blue sticks correspond to singlet channels, while green sticks correspond to triplet channels.

when moving from high to low electron kinetic energy (see the upper panel of Fig. 5), with peak maxima located around 250.0 eV, 237.5 eV, and 229.6 eV. Similar to H_2O , the three peaks represent transitions to doubly ionized states with holes in either (1) the outer valence shell only, (2) both outer and inner valence shells, or (3) the inner valence shell only, with the first case yielding the largest intensity.

Table V and Fig. 5 show the results of our calculations of Auger spectra for CH₄. The Coulomb wave effective charge of 3.6 is based on the Slater rules applied to an isolated C atom. Just as with Ne and H₂O, the main effect of the Coulomb wave is the reduction of the intensity in the triplet T₂ channel, which is considerably overestimated by the plane wave model. The model with the Coulomb wave reproduces all main features of the spectrum quite well; however, there is still an imbalance between the intensities for the singlet decay channels. Our model also neglects the contributions from the shake-up satellite transitions, which affect the spectrum in the region around 240–250 eV. 73

For the total one-electron K–LL Auger width, our models with the plane wave and Coulomb wave predict 95.0 meV and 66.8 meV, respectively. These total widths include contributions from all EOM-CC channels down to 228 eV. Direct comparison with the experimentally determined natural linewidth of the $1a_1^{-1}$ core–hole state in CH₄ is more difficult, as values reported from different measurements vary significantly, ranging from 83 \pm 10 meV to 120 \pm 10 meV. Nevertheless, it is clear that the model with the Coulomb wave tends to underestimate the total width, while the model with the plane wave gives a better estimate of the total width, likely as a consequence of a fortuitous error cancellation.

D. CO_2 (C-edge $1s^{-1}$)

 CO_2 is another small molecule being extensively used for benchmark studies in core-level spectroscopies. It has two distinct K-LL Auger spectra due to ionization from either carbon or oxygen K-shell, and both have been reported and scrutinized several times. ^{62,78-83} Here, we focus only on the carbon K-LL Auger spectrum, as due to symmetry, we can apply our models for the continuum electron in a straightforward manner. Outside the K-shell,

TABLE V. Energies (in eV), total (Γ_{tot}) and partial (Γ_i) widths (in meV) for the main channels in the Auger decay of *K*-shell ionized methane. Calculations of the widths used either a plane wave or a Coulomb wave with effective charge Z_{eff} = 3.6 for all channels.

		Γ_i (meV)		
Channel	Energy (eV)	$\overline{Z_{eff}} = 0$	$Z_{eff} = 3.6$	
$^{3}T_{1}$	252.27	0.1	0.0	
¹ E	251.59	17.0	10.7	
$^{1}T_{2}$	250.22	24.7	16.0	
$^{1}A_{1}$	248.36	0.6	6.0	
$^{3}T_{2}$	243.23	42.1	6.8	
$^{1}T_{2}$	237.63	2.5	14.2	
$^{1}A_{1}$	229.73	8.0	13.1	
$\Gamma_{ m tot}$		95.0	66.8	

the electronic configuration of CO₂ in the ground state is given as follows: $(3\sigma_g^2)(2\sigma_u^2)(4\sigma_g^2)(3\sigma_u^2)(1\pi_u^4)(1\pi_g^4)$. It has a much larger number of possible channels with two hole vacancies in the valence shell than H₂O and CH₄. The experimental Auger spectrum from the carbon K-edge, shown in the upper panel of Fig. 6, has most of its intensity gathered in the two largest peaks around 250 eV. There are also two pronounced sharp peaks at a higher kinetic energy (254-258 eV) and a series of much broader peaks at lower energies from 245 eV to 225 eV. Table VI and Fig. 6 show the computed Auger spectra. In the calculations with the Coulomb wave, we assumed the effective charge of 3.6 (same as in CH₄), centered on the carbon atom. The convergence pattern of the pseudo-wave expansion of the Coulomb wave for selected channels in CO₂ is illustrated in the supplementary material. As one can see, both of our models reproduce the experimental spectrum quite well, and the predicted relative intensities and positions of the peaks allow for unique assignment of the observed features in the spectrum. Interestingly, even with the simplest model of the plane wave, the overall shape of the spectrum is as good as in the model with the Coulomb wave. However, the analysis of Table VI clearly shows that the plane wave orbital largely overestimates the contributions

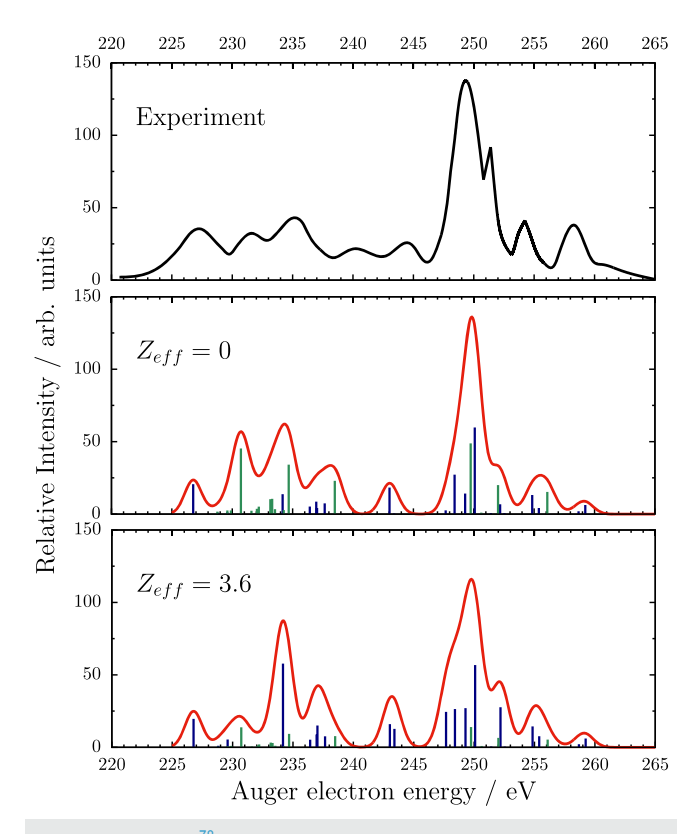


FIG. 6. Experimental 78 and computed Auger spectra for carbon K-edge in CO_2 . Middle and bottom panels show the calculations with a plane wave and a Coulomb wave, respectively. Theoretical curves obtained from the stick spectra by assuming a constant Gaussian broadening of 0.7 eV FWHM. Dark-blue sticks correspond to singlet channels, while green sticks correspond to triplet channels, respectively.

TABLE VI. Energies (in eV), total (Γ_{tot}) and partial (Γ_i) widths (in meV) for the main channels in the Auger decay of carbon-edge K-shell ionized CO₂. Calculations of the widths used either a plane wave or a Coulomb wave with effective charge Z_{eff} = 3.6 for all channels.

		Γ_i (meV)		
Channel	Energy (eV)	$\overline{Z_{eff}} = 0$	$Z_{eff} = 3.6$	
$^{-1}\Delta_{g}(1\pi_{g}^{-2})$	259.23	1.0	0.7	
$^{1}\Sigma_{g}^{+}(1\pi_{g}^{-2})$	258.68	0.3	0.2	
$^{3}\Pi_{u}(1\pi_{g}^{-1}3\sigma_{u}^{-1})$	256.09	2.5	0.6	
$^{1}\Pi_{u}(1\pi_{g}^{-1}3\sigma_{u}^{-1})$	255.39	0.7	0.8	
$^{1}\Pi_{g}(1\pi_{g}^{-1}4\sigma_{g}^{-1},1\pi_{u}^{-1}3\sigma_{u}^{-1})$	254.84	2.2	1.6	
$^{1}\Sigma_{g}^{+}(3\sigma_{u}^{-2},4\sigma_{g}^{-2})$	252.18	1.1	3.1	
$^{3}\Sigma_{u}^{+}(4\sigma_{g}^{-1}3\sigma_{u}^{-1})$	252.01	3.3	0.7	
$^{1}\Delta_{g}(1\pi_{u}^{-2})$	250.08	10.0	6.3	
$^{3}\Pi_{u}(4\sigma_{g}^{-1}1\pi_{u}^{-1})$	249.75	8.1	1.6	
$^{1}\Sigma_{\sigma}^{+}(1\pi_{u}^{-2})$	249.28	2.4	3.0	
$^{1}\Pi_{g}^{0}(3\sigma_{u}^{-1}1\pi_{u}^{-1},4\sigma_{g}^{-1}1\pi_{g}^{-1})$	248.41	4.5	2.9	
$^{1}\Pi_{u}(4\sigma_{g}^{-1}1\pi_{u}^{-1},3\sigma_{u}^{-1}1\pi_{g}^{-1})$	247.67	0.4	2.7	
$^{1}\Sigma_{u}^{+}(4\sigma_{g}^{-1}3\sigma_{u}^{-1})$	243.40	0.1	1.4	
$^{1}\Sigma_{g}^{+}(4\sigma_{g}^{-2},3\sigma_{u}^{-2})$	243.02	3.0	1.8	
$^{3}\Pi_{u}(2\sigma_{u}^{-1}1\pi_{g}^{-1})$	238.49	3.8	0.9	
$^{1}\Pi_{u}(2\sigma_{u}^{-1}1\pi_{g}^{-1})$	237.02	0.7	1.7	
$^{3}\Sigma_{u}^{+}(3\sigma_{g}^{-1}3\sigma_{u}^{-1},4\sigma_{g}^{-1}2\sigma_{u}^{-1})$	234.67	5.7	1.0	
$^{1}\Sigma_{g}^{+}(2\sigma_{u}^{-1}3\sigma_{u}^{-1},3\sigma_{g}^{-1}4\sigma_{g}^{-1})$	234.17	2.3	6.4	
$^{3}\Pi_{u}(3\sigma_{g}^{-1}1\pi_{u}^{-1})$	230.72	7.6	1.5	
$^{1}\Pi_{g}(2\sigma_{u}^{-1}1\pi_{u}^{-1},3\sigma_{g}^{-1}1\pi_{g}^{-1})$	226.77	3.4	2.2	
$\Gamma_{ m tot}$		76.1	48.9	

from the triplet channels, the behavior observed in other studied molecules. At the same time, the overestimated triplet channels are located energetically relatively close to the singlet channels, which are truly populated in the Auger decay. Therefore, even though the exact assignment of the peaks based on the calculations with the plane wave can be incorrect, the total shape of the spectrum might turn out surprisingly well, particularly for larger molecules with many accessible final states contributing to the observed signal. As shown above, also for CO2, the Coulomb wave reverses the Auger transition intensities from triplet to singlet channels. Interestingly, the Coulomb wave also performs quite well for the channels with highest kinetic energy dominated by two vacancies in the highest occupied molecular orbital, $1\pi_g$, which, for symmetry reasons, does not contain carbon character. Overall, the Coulomb wave permits the interpretation of the main features in the CO2 Auger spectrum, which agrees very well with the previously published results based on ADC(2) calculations and the atomic two-hole population analysis. 78,79,81 The main discrepancy from the measured spectrum occurs around the region with two relatively broad peaks centered at around 244 eV and 240 eV. In this region, our EOM-DIP calculations yield two almost degenerate channels ($^{1}\Sigma_{u}^{+}$ and $^{1}\Sigma_{g}^{+}$), with an energy difference of only 0.4 eV and centered at 243 eV. One important aspect, which is neglected in our study, is nuclear dynamics and broadening of the Auger spectrum due to the vibrational structure in the initial and final states. Theoretical spectra depicted in Fig. 6 assumed a fixed Gaussian profile with the FWHM of $0.7~{\rm eV}$. This is a crude approximation, given that the fits to the experimental spectrum yielded the widths of the peaks varying from $0.3~{\rm eV}$ up to a few eV. The effect of the nuclear dynamics contributes also to the shift of the peaks relative to the vertical Auger transitions assumed in our work.

For the total one-electron Auger decay rate, our models yield 76.1 meV and 48.9 meV for the plane wave and the Coulomb wave continuum orbitals, respectively. Reported experimental widths for the C $1s^{-1}$ state of CO2 vary between 70 meV and 100 meV. $^{84-86}$ The underestimation of the total width should be attributed mostly to the fact that our calculations neglect the contributions from the lower energy range of the Auger spectrum (below 226 eV) where numerous doubly excited states contribute considerably to the state lifetime.

E. Ne $(1s^{-1}3p)$

In the resonant Auger process, the initial state for autoionization is created by a resonant excitation of a core electron to

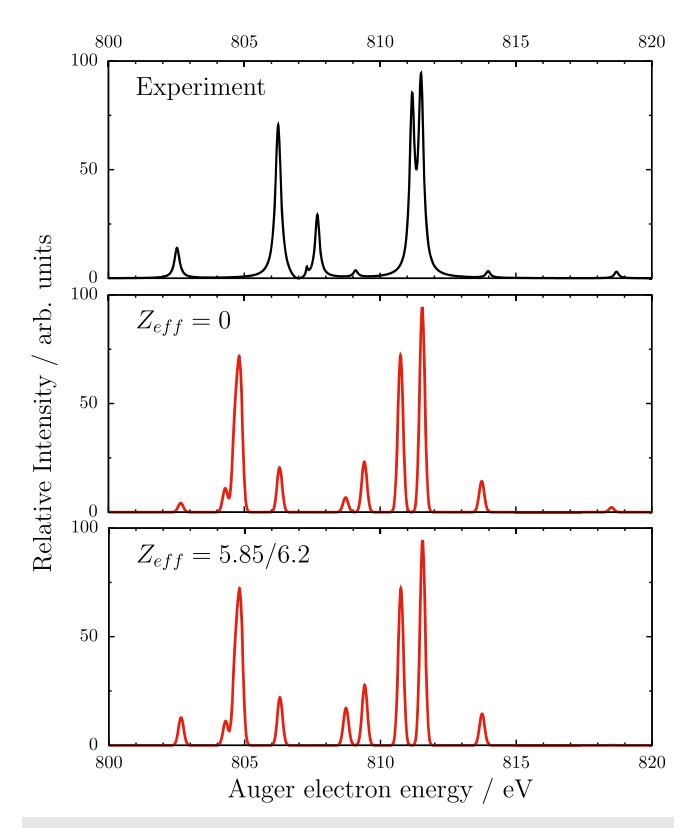


FIG. 7. Experimental⁶⁹ and computed resonant Auger spectra following $1s \rightarrow 3p$ transition in the Ne atom. The middle and bottom panels show calculations with a plane wave and a Coulomb wave, respectively. Theoretical curves were obtained from the stick spectra by a assuming constant Gaussian broadening of 0.1 eV FWHM and normalized to the height of the dominant 2F channel. All theoretical peaks corresponding to spectator-type transitions were shifted by 10.1 eV to match the position of the experimental 2F channel.

a vacant valence orbital (see Fig. 1). Due to the coupling between the excited electron and the remaining core, there is a significant increase in the number of possible decay channels compared to the regular Auger process. Additionally, a more diffuse character of the initial core-excited state makes shake-up and shake-down processes more pronounced. Therefore, the resonant Auger spectra have more complicated patterns and pose a greater challenge to theory. As the first example here, we consider the Auger decay following the $1s \rightarrow 3p(^{1}P_{1})$ excitation in the Ne atom. The relaxation of the $1s^{-1}3p^{1}$ P₁ state proceeds via multiple autoionization (Auger cascade), with one Auger electron ejected after another. 89-91 Here, we consider only the first step of this process in which singly charged Ne⁺ ions are formed. The top panel in Fig. 7 shows the experimental Auger emission spectrum of $1s^{-1}3p^{1}$ Ne, covering the energy range from 800 eV to 820 eV, where most of the intensities are located. There are three main classes of Auger processes occurring in the decay of $1s^{-1}3p^1$ Ne: (a) spectator processes of the type $1s2s^22p^63p \rightarrow 1s^2(2s2p)^63p + e^-$, where the initially excited electron does not participate in the autoionization, (b) shake-up processes of the type $1s2s^22p^63p \rightarrow 1s^2(2s2p)^64p + e^-$, where there is additional excitation to the higher Rydberg level, and (c) participator processes of the type $1s2s^22p^63p \rightarrow 1s^2(2s2p)^7 + e^-$, where the electron from the Rydberg orbital participates directly in the autoionization. From the previous studies, it is well known that the decay of the $1s^{-1}3p^1$ state is dominated by the spectator processes. The highest peaks in Fig. 7 can be assigned to channels with Ne⁺ valence configurations of $2s^22p^4(^1D)3p$. There are also significant contributions from shake-up transitions with the final valence configurations of $2s^22p^4(^1D)4p$, while participator processes are the least important.

Table VII shows the results of our calculations compared with available experimental data. Here, we employ the fully uncontracted d aug-cc-pVTZ basis set to describe the Rydberg-like 3*p*/4*p* orbitals.

As far as channel energies are considered, our computational model describes well only the participator channels and performs rather poorly for the spectator or shake-up transitions, which are blueshifted by around 10 eV, despite using a one-electron basis set with additional diffuse functions. As the initial excitation energy for 1s \rightarrow 3p transition is well reproduced in our model (866.86 eV vs the experimental value of 867.13 eV), the underestimated channel energies are the consequence of a poor description of Ne⁺ excited Rydberg states. When the closed-shell Ne atom serves as a reference state for the EOM-CC calculations, Ne+ excited states dominated by configurations such as $1s^2(2s2p)^63p$ or $1s^2(2s2p)^64p$ can only be obtained by means of double excitations (i.e., 2h1p configurations from Fig. 1) or higher. Therefore, due to the lack of 3h2p excitations in the EOM-IP-CCSD model, these states are described less accurately than the states of 1h character. The resulting insufficient description of correlation and relaxation effects results in ~10 eV errors.

As in the above examples, we computed Auger partial widths with either a plane wave or Coulomb wave to model the continuum electron. For the Coulomb wave, the chosen effective charge Z = 5.85 for participator channels and Z = 6.2 for spectator channels (it is assumed that screening by the spectator electron is negligible). To facilitate the comparison of the computed Auger intensities with the experimental data, the theoretical spectra shown in Fig. 7 were obtained in such a way that all peaks due to the channels with an occupied Rydberg level have been shifted by 10.1 eV in order to match the experimental position of the most intense peak at 811.5 eV, which is due to the ${}^{2}F(2s^{2}2p^{4}({}^{1}D)3p^{1})$ channel. Additionally, theoretical spectra have been normalized to the height of the dominant peak, and a constant broadening of 0.1 eV with a Gaussian envelope has been introduced. The agreement between the calculated and experimental spectra is only qualitative. Our calculations correctly describe the relative intensities of the most

TABLE VII. Energies (in eV), total (Γ_{tot}) and partial (Γ_i) widths (in meV), and relative intensities I_i for the Auger decay of the 1s \to 3p core-excited Ne atom from present calculations compared with experimental data. Calculations of the widths used either a plane wave or a Coulomb wave with effective charge Z_{eff} = 5.85 for 1h-type channels and Z_{eff} = 6.2 for 2h1p-type channels. Relative intensities I_i are given in % with respect to the intensity of the dominant 2F channel.

Channel	Energy (eV)		Γ_i (meV)		I_i		
	Present	Expt. ⁸⁷	$\overline{Z_{eff}} = 0$	$Z_{eff} = 5.85/6.2$	$Z_{eff}=0$	$Z_{eff} = 5.85/6.2$	Expt.88
${}^{2}P(2s^{2}2p^{5})$	845.52	845.47	1.0	0.7	2.3	2.4	
$^{2}S(2s^{1}2p^{6})$	818.39	818.56	1.0	0.02	2	0.1	
$^{2}P(2s^{2}2p^{4}(^{3}P)3p^{1})$	803.65	814.04	6.6	4.5	15	15	3
${}^{2}\text{F}(2s^{2}2p^{4}({}^{1}\text{D})3p^{1})$	801.46	811.54	43.5	29.2	100	100	100
$^{2}D(2s^{2}2p^{4}(^{1}D)3p^{1})$	800.66	811.18	33.3	22.4	76	76	73
$^{2}P(2s^{2}2p^{4}(^{1}D)3p^{1})$	799.33	811.28	10.7	8.6	25	29	37
$^{2}P(2s^{2}2p^{4}(^{3}P)4p^{1})$	798.64	809.07	3.1	5.3	7	18	
$^{2}P(2s^{2}2p^{4}(^{1}S)3p^{1})$	796.21	807.70	9.5	6.8	22	23	32
$^{2}\text{F}(2s^{2}2p^{4}(^{1}\text{D})4p^{1})$	794.75	806.28	29.2	19.7	67	67	
$^{2}D(2s^{2}2p^{4}(^{1}D)4p^{1})$	794.57	806.17	18.2	12.3	42	42	
$^{2}P(2s^{2}2p^{4}(^{1}D)4p^{1})$	794.21	806.16	5.0	3.4	12	12	
$^{2}P(2s^{2}2p^{4}(^{1}S)4p^{1})$	792.57	802.52	2.0	4.0	4	14	
$\Gamma_{ m tot}$			163.6	117.3			

pronounced transitions; however, there is a mismatch in the positions and intensities of the satellite peaks. Relative intensities obtained with the plane wave and the Coulomb wave are almost identical, while there is a significant reduction in the absolute widths when the Coulomb wave is employed. This behavior can be related to the fact that the vast majority of the probed decay channels have $2s^22p^4(^1D)3p/4p$ configurations, which are associated with the emission of the d-wave electron. As we have seen in the case of regular Auger decay for the $2s^22p^4(^1D)$ channel (d-wave emission), using the Coulomb wave with an effective charge of Z_{eff} = 6.2 reduces the Auger intensity by ~1/3 relative to the plane wave calculation (see Fig. 2 and Table II). Here, the performance is the same because the Rydberg electron from the 3p/4p orbital is not expected to impact significantly short-range electronic density near the nucleus, which is important for the Auger process. Within the same electronic configurations, the relative Auger intensities are mostly determined by geometrical and symmetry factors (state degeneracy), and therefore, they remain largely unaffected by the change in the form of the employed scattered wave. Similar behavior of the absolute and relative Auger intensities for these transitions has been observed in recent ab initio calculations based on the RASSCF wave

Our estimates of the total width are 163.6 meV and 117.3 meV based on the plane wave and Coulomb-wave continuum orbital, respectively. These numbers are significantly below the most-recent experimental determination of the natural linewidth of the Ne $(1s^{-1}3p)$ level, which is $248 \pm 2.^{48}$ Our calculations, however, cover the channels from the energy range down to 780 eV, thus neglecting significant contribution to the total width from the p-wave region between 770 eV and 780 eV.

F. CO₂ (C-edge, $1s \rightarrow \pi^*$)

To assess the performance of our model for molecular resonant Auger decay, we chose the C-edge core-excited $1s \to \pi_u^*(^1\Pi_u)$ transition in CO₂ as a test case. This state has been thoroughly investigated and has proven to be challenging for precise computational modeling due to both geometrical effects and the complex pattern of possible decay channels. ^{94–97} In particular, the Renner–Teller effect in the core-excited $^1\Pi_u$ state makes the Auger spectra highly sensitive to the exact excitation energy. ⁹⁸ After the degeneracy of the $^1\Pi_u$ state is lifted for the bent geometry, two overlapping resonant states appear, and non-adiabatic quantum-dynamical calculations are required to properly account for possible vibrational and electronic interferences.

The measured resonant electron Auger spectrum following C $1s \rightarrow \pi_u^*(^1\Pi_u)$ excitation in CO_2 is shown in the uppermost panel of Fig. 8. Previous theoretical studies utilizing comparisons with valence photoionization and normal Auger spectra delivered a satisfactory interpretation of the resonant Auger CO_2 . The region above the electron kinetic energy of 270 eV (a binding energy of less than 20 eV) is exclusively due to the participator transitions to CO_2^+ states with one hole in the orbital from the outer valence shell $(1\pi_g^{-1}, 1\pi_u^{-1}, 3\sigma_u^{-1}, \text{ or } 4\sigma_g^{-1})$. Additional contributions from the participator-like transitions to states with a single hole in the inner valence shell $(2\sigma_u^{-1} \text{ or } 3\sigma_g^{-1})$ are located between 250 eV and 255 eV (with the binding energy of 35–40 eV). The rest of the spectrum, including all peaks with the electron kinetic energy between 255 eV and 270 eV,

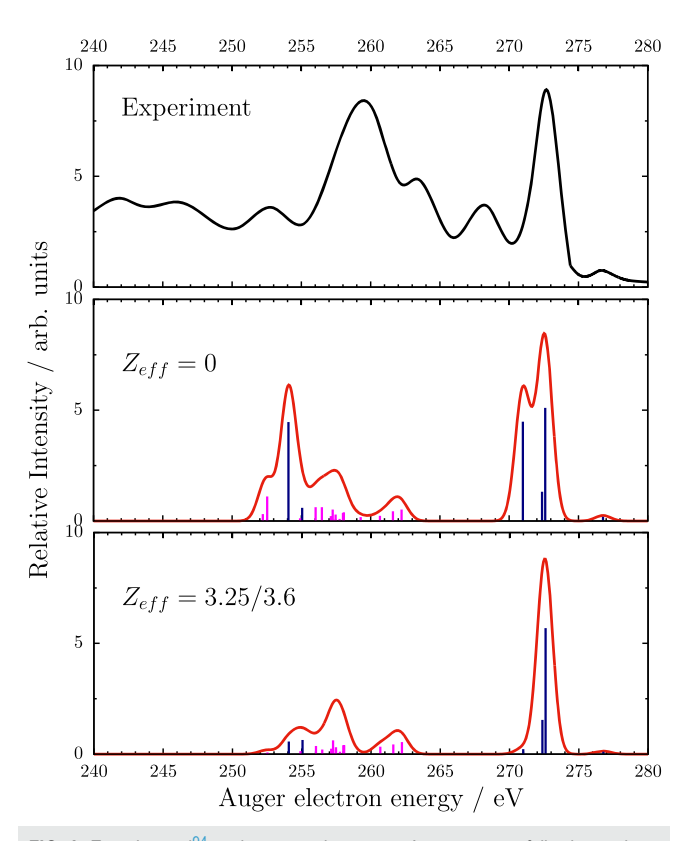


FIG. 8. Experimental 94 and computed resonant Auger spectra following carbonedge $1s \to \pi^*_u$ excitation in CO $_2$. Middle and bottom panels show the calculations with a plane wave and a Coulomb wave, respectively. Theoretical curves are obtained from the stick spectra by assuming a constant Gaussian broadening of 0.7 eV FWHM. Dark-blue sticks represent participator channels, while magenta sticks are spectator channels.

can be assigned to the spectator decay, where the final CO_2^+ states have dominant configurations with two holes in the valence shell and the excited electron in the π_u^+ orbital.

Table VIII and Fig. 8 show the results of our calculations. Similar to the resonant Auger spectrum in Ne, for the model with the Coulomb wave, we applied two different effective charges: $Z_{eff} = 3.25$ for participator channels and $Z_{eff} = 3.6$ for spectator channels, which are derived from Slater rules applied to the isolated C atom with the assumption that the electron from the outer π_u^* orbital does not contribute to the screening. Our theoretical spectra only partly reproduce the experimental features. Clearly, our estimates are more accurate for participator channels than for spectator channels. Our models correctly identify the highest peak due to the ${}^2\Pi_u(\pi_u^{-1})$ state. Also the relative intensities and positions of the other participator channels are reproduced reasonably well. The model with the Coulomb wave does a better job, as the plane wave overestimates the intensities of the two ${}^2\Sigma_g^+$ participator states. Our calculations fail with regard to the spectator channels. In our model, the onset of spectator channels appears at around 262 eV (a binding energy of 28 eV), while that in the measured spectrum is around 268 eV (a binding energy of 22 eV). As in the Ne case, this error can be

TABLE VIII. Energies (in eV), total (Γ_{tot}) and partial (Γ_i) widths (in meV) for the main channels in the Auger decay of 1s $\to \pi^*$ C-edge core-excited CO $_2$ from the present calculations. Calculations of the widths used either a plane wave or a Coulomb wave with effective charge $Z_{eff}=3.25$ for 1h-type channels and $Z_{eff}=3.6$ for 2h1p-type channels. Calculations of the total width Γ_{tot} include channels with an Auger electron energy down to 250 eV.

		Г	(meV)
Channel	Energy (eV)	$Z_{eff}=0$	$Z_{eff} = 3.25/3.6$
$^{2}\Pi_{g}(1\pi_{g}^{-1})$	276.77	0.4	0.14
$^{2}\Pi_{u}(1\pi_{u}^{-1})$	272.60	10.2	7.1
$^{2}\Sigma_{u}^{+}(3\sigma_{u}^{-1})$	272.37	2.6	1.9
$^2\Sigma_g^+(4\sigma_g^{-1})$	270.99	9.0	0.3
$^{2}\Sigma_{u}^{+}(2\sigma_{u}^{-1})$	255.06	1.2	0.8
$^{2}\Sigma_{g}^{+}(3\sigma_{g}^{-1})$	254.07	8.9	0.7
$^{2}\Pi_{u}(1\pi_{g}^{-2}\pi_{u}^{*},1\pi_{u}^{-2}\pi_{u}^{*})$	262.23	1.0	0.7
$^{2}\Pi_{u}(1\pi_{g}^{-2}\pi_{u}^{*},1\pi_{u}^{-2}\pi_{u}^{*})$	261.61	0.9	0.5
$^{2}\Pi_{u}(1\pi_{u}^{-2}\pi_{u}^{*},1\pi_{u}^{-2}\pi_{u}^{*})$	260.67	0.5	0.4
$^{2}\Sigma_{g}^{+}(1\pi_{g}^{-2}\sigma_{g}^{*})$	259.28	0.4	0.02
$\begin{array}{c} ^{2}\Sigma_{g}^{+}(1\pi_{g}^{-2}\sigma_{g}^{*}) \\ ^{2}\Sigma_{g}^{+}(1\pi_{g}^{-1}3\sigma_{u}^{-1}\pi_{u}^{*}) \end{array}$	258.06	0.8	0.5
$^{2}\Sigma_{u}^{+}(1\pi_{\sigma}^{-1}4\sigma_{\sigma}^{-1}\pi_{u}^{*},1\pi_{u}^{-1}3\sigma_{u}^{-1}\pi_{u}^{*})$	258.00	0.7	0.5
$^{2}\Sigma_{u}^{-}(1\pi_{u}^{s-1}1\pi_{g}^{s-1}\sigma_{g}^{*})$	257.76	0.2	0.1
$^{2}\Sigma_{u}^{+}(1\pi_{u}^{-1}1\pi_{\sigma}^{-1}\sigma_{\sigma}^{*})$	257.47	0.6	0.4
$\begin{array}{cccccccccccccccccccccccccccccccccccc$	257.47	0.1	0.2
$^{2}\Sigma_{g}^{-}(1\pi_{g}^{-1}3\sigma_{u}^{-1}\pi_{u}^{*})$	257.34	0.1	0.1
$^{2}\Pi_{\nu}(1\pi_{\alpha}^{-2}\pi_{\nu}^{*},1\pi_{\alpha}^{-1}3\sigma_{\nu}^{-1}\sigma_{\alpha}^{*})$	257.26	1.0	0.8
$\begin{array}{cccccccccccccccccccccccccccccccccccc$	257.13	0.4	0.3
$^{2}\Sigma_{g}^{-}(1\pi_{u}^{-1}4\sigma_{g}^{-1}\pi_{u}^{*})$	256.48	1.2	0.3
$^{2}\Sigma_{g}^{-}(1\pi_{u}^{-1}4\sigma_{g}^{-1}\pi_{u}^{*})$	256.03	1.2	0.5
$\begin{array}{l} {}^{2}\Sigma_{g}^{g}\left(1\pi_{u}^{-1}4\sigma_{g}^{g-1}\pi_{u}^{*}\right) \\ {}^{2}\Pi_{u}\left(1\pi_{g}^{-1}3\sigma_{u}^{-1}\sigma_{g}^{*},1\pi_{u}^{-1}4\sigma_{g}^{-1}\sigma_{g}^{*}\right) \end{array}$	254.91	0.2	0.2
$^{2}\Sigma_{g}^{+}(1\pi_{g}^{-2}\sigma_{g}^{*},1\pi_{g}^{-1}3\sigma_{u}^{-1}\pi_{u}^{*})$	252.53	2.2	0.1
${2 \sum_{g}^{+} (1 \pi_{g}^{-2} \sigma_{g}^{*}, 1 \pi_{g}^{-1} 3 \sigma_{u}^{-1} \pi_{u}^{*}) \atop 2 \sum_{u}^{+} (1 \pi_{g}^{-1} 4 \sigma_{g}^{-1} \pi_{u}^{*}, 1 \pi_{u}^{-1} 3 \sigma_{u}^{-1} \pi_{u}^{*})}$	252.50	0.1	0.1
$^{2}\Sigma_{g}^{+}(1\pi_{g}^{-1}3\sigma_{u}^{-1}\pi_{u}^{*})$	252.22	0.6	0.03
$\Gamma_{ m tot}$		45.0	18.2

traced back to the limited ability of the EOM-IP-CCSD ansätze to describe the excited states of the 2h1p type. In addition to the mismatch in the position, the relative intensities of the spectator channels are also not reproduced well. One would expect that the spectator channels would show a pattern that closely resembles the regular Auger spectrum (Fig. 6) but is shifted to higher kinetic energy by ~9.7 eV. However, this pattern is not well reproduced by either the plane wave or the Coulomb-wave model, with both models possibly significantly underestimating the Auger transitions from spectator states.

When comparing the spectra obtained with the plane wave and the Coulomb wave, we observe that the main difference appears for the $^2\Sigma_g^+$ channels of both the participator and spectator types, which are reduced by roughly one order of magnitude when employing the Coulomb wave. The Coulomb wave likely provides an improvement over the plane wave, as it is known from vibrationally resolved Auger

spectra in the participator region that the intensities of the $^2\Sigma_g^+$ channels are much lower than of the $^2\Pi_u$ channel. At the same time, employing the Coulomb wave does not seem to affect most spectator channels and their overall contribution to the Auger spectra. This can be rationalized by the fact that in the region with a high density of final states with strongly mixed configurations, details due to the exact shape of the continuum orbital are averaged out. Also, this behavior for spectator channels is consistent with the results for the regular Auger spectrum (Fig. 6), where the plane wave and the Coulomb wave performed nearly the same.

IV. CONCLUSIONS AND OUTLOOK

We have presented numeric results illustrating the performance of the extension of the EOM-CCSD formalism²⁸ to the computation of Auger decay rates in atoms and molecules. We calculated Auger decay rates using the Feshbach-Fano formalism, with manyelectron EOM-CC states and a continuum orbital describing the outgoing electron approximated by either a plane wave or a Coulomb wave. Our benchmark calculations for the Ne atom and H₂O, CH₄, and CO₂ molecules show that, despite their simplicity, these models for the continuum orbital are able to treat the autoionization of core-exited and core-ionized states reliably and can be used to explain experimental spectra. The variant with the plane wave is particularly easy to apply, as it is parameter-free and affords fast calculations, even with sizable orbital basis sets. This model can be considered as an extension of statistical approaches 100,101 that partially accounts for the scattering character of the Auger decay and for the symmetry of the initial and final states. It also provides lowest-order estimation of partial and total transition rates. When applying moresophisticated models for the continuum orbitals, calculations with a pure plane wave can be used for fast initial screening of decay channels in order to identify those that are important for the given system. Furthermore, due to the localized nature of the Auger process, the higher the partial waves contributing to the decay are, the more accurate the estimation based on the plane wave approximation is expected to be.

Plane-wave description of the continuum orbital has its limitations, and our calculations have shown that this model fails to describe branching ratios between the singlet and triplet channels resulting from the same orbital occupations. This deficiency is rectified by using a Coulomb wave instead of a plane wave. Application of the Coulomb wave requires specification of its effective charge and the origin. The effective charge can be chosen based on different criteria; here, we have mostly tested the effective charges resulting from Slater rules applied to an isolated atom bearing the core vacancy. In this way, our Coulomb wave model is closely related to the commonly used one-center approximation with pure atomic continuum functions. In general, we observed that application of the Coulomb wave, even with a simple choice of the effective charge based on Slater rules, improves the partial decay widths, particularly for regular Auger decay in cases when both singlet and triplet channels are possible. At the same time, the results for CO₂ do not differ significantly between the plane wave and Coulombwave models. This is mainly because of the larger density of possible decay channels than in smaller systems such as Ne or H₂O and the overall effect of averaging when there are multiple closely

spaced channels contributing to the spectrum. Therefore, we anticipate that in more complex molecules, the differences between plane wave and Coulomb wave will be reduced. This observation might be helpful in investigations of environment effects on the Auger lifetime.

Certainly, the present work does not discuss the full complexity of the problem, and there are important issues that remain to be addressed to improve the predictive power of the methodology. First, a more realistic description of the continuum orbital should be obtained by solving the mean-field problem. A natural basis set to calculate the continuum orbital would be products of the Gaussian and plane wave functions, which would keep the calculations of all integrals fully analytic. Second, the importance of the inter-channel coupling should be explored, and some way to estimate its contribution in molecules should be proposed. Third, to improve the description of resonant Auger decay, it is necessary to include the triple excitation operator in the EOM-CC ansätze. Full EOM-CCSDT calculations might be limited to rather small systems; however, approximate models 102,103 might be sufficient to reduce the error in the description of the satellite and spectator channels. Finally, the complete treatment of Auger electron spectra in molecules should include the effect of Franck-Condon broadening and vibrational dynamics.

SUPPLEMENTARY MATERIAL

See the supplementary material for the study of the orbital basis-set dependence of Auger widths in the Ne atom, convergence of pseudo-partial wave expansion in CO_2 , norms of two-body Dyson functions in the Auger decay of H_2O , and optimized geometries of the studied molecules.

ACKNOWLEDGMENTS

This work was supported by the U.S. National Science Foundation (Grant No. CHE-1856342). We thank Dr. Evgeny Epifanovsky from Q-Chem, Inc., and Dr. Pavel Pokhilko for their help and guidance in the implementation of mixed Gaussian-plane wave integrals. A.I.K. is the president and a part-owner of Q-Chem, Inc.

DATA AVAILABILITY

The data that support the findings of this study are available within the article and its supplementary material.

REFERENCES

- ¹X-Ray Absorption and X-Ray Emission Spectroscopy; Theory and Applications, edited by J. A. van Bokhoven and C. Lamberti (Wiley & Sons, Chichester, Germany, 2016).
- ² Synchrotron Radiation: Basics, Methods and Applications, edited by S. Mobilio, F. Boscherini, and C. Meneghini (Springer, Berlin, Germany, 2014).
- ³X-Ray Free Electron Lasers: Applications in Materials, Chemistry and Biology, Number 18 in Energy and Environment Series, edited by U. Bergmann, V. K. Yachandra, and J. Yano (Royal Society of Chemistry, Croydon, UK, 2017).
- ⁴M. Nisoli, P. Decleva, F. Calegari, A. Palacios, and F. Martín, "Attosecond electron dynamics in molecules," Chem. Rev. 117, 10760 (2017).
- ⁵P. Norman and A. Dreuw, "Simulating X-ray spectroscopies and calculating core-excited states of molecules," Chem. Rev. 118, 7208 (2018).

- ⁶O. Kostko, B. Bandyopadhyay, and M. Ahmed, "Vacuum ultraviolet photoionization of complex chemical systems," Annu. Rev. Phys. Chem. **67**, 19 (2016).
- ⁷L. S. Cederbaum, W. Domcke, and J. Schirmer, "Many-body theory of core holes," Phys. Rev. A 22, 206 (1980).
- ⁸A. I. Krylov, "Equation-of-motion coupled-cluster methods for open-shell and electronically excited species: The Hitchhiker's guide to Fock space," Annu. Rev. Phys. Chem. **59**, 433 (2008).
- ⁹J. F. Stanton and R. J. Bartlett, "The equation of motion coupled-cluster method. A systematic biorthogonal approach to molecular excitation energies, transition probabilities, and excited state properties," J. Chem. Phys. **98**, 7029 (1993)
- ¹⁰R. J. Bartlett, "Coupled-cluster theory and its equation-of-motion extensions," Wiley Interdiscip. Rev.: Comput. Mol. Sci. 2, 126 (2012).
- ¹¹K. Sneskov and O. Christiansen, "Excited state coupled cluster methods," Wiley Interdiscip. Rev.: Comput. Mol. Sci. 2, 566 (2012).
- ¹²S. Coriani and H. Koch, "Communication: X-ray absorption spectra and core-ionization potentials within a core-valence separated coupled cluster framework," J. Chem. Phys. **143**, 181103 (2015).
- ¹³S. Coriani and H. Koch, "Erratum: 'Communication: X-ray absorption spectra and core-ionization potentials within a core-valence separated coupled cluster framework' [J. Chem. Phys. 143, 181103 (2015)]," J. Chem. Phys. 145, 149901 (2016).
- ¹⁴M. L. Vidal, X. Feng, E. Epifanovsky, A. I. Krylov, and S. Coriani, "A new and efficient equation-of-motion coupled-cluster framework for core-excited and core-ionized states," J. Chem. Theory Comput. 15, 3117 (2019).
- ¹⁵M. L. Vidal, A. I. Krylov, and S. Coriani, "Dyson orbitals within the fc-CVS-EOM-CCSD framework: Theory and application to X-ray photoelectron spectroscopy of ground and excited states," Phys. Chem. Chem. Phys. 22, 2693 (2020).
- ¹⁶R. Faber and S. Coriani, "Resonant inelastic X-ray scattering and nonesonant X-ray emission spectra from coupled-cluster (damped) response theory," J. Chem. Theory Comput. 15, 520 (2019).
- ¹⁷K. D. Nanda, M. L. Vidal, R. Faber, S. Coriani, and A. I. Krylov, "How to stay out of trouble in RIXS calculations within the equation-of-motion coupled-cluster damped response theory framework? Safe hitchhiking in the excitation manifold by means of core-valence separation," Phys. Chem. Chem. Phys. 22, 2629 (2020).
- ¹⁸R. Faber and S. Coriani, "Core-valence-separated coupled-cluster-singles-and-doubles complex-polarization-propagator approach to X-ray spectroscopies," Phys. Chem. Chem. Phys. 22, 2642 (2020).
- ¹⁹K. D. Nanda and A. I. Krylov, "A simple molecular orbital picture of RIXS distilled from many-body damped response theory," J. Chem. Phys. **152**, 244118 (2020).
- ²⁰ K. D. Nanda and A. I. Krylov, "Cherry-picking resolvents: A general strategy for convergent coupled-cluster damped response calculations of core-level spectra," J. Chem. Phys. 153, 141104 (2020).
- ²¹ M. L. Vidal, P. Pokhilko, A. I. Krylov, and S. Coriani, "Equation-of-motion coupled-cluster theory to model L-edge x-ray absorption and photoelectron spectra," J. Phys. Chem. Lett. 11, 8314 (2020).
- ²² M. L. Vidal, A. I. Krylov, and S. Coriani, "Correction: Dyson orbitals within the fc-CVS-EOM-CCSD framework: Theory and application to X-ray photoelectron spectroscopy of ground and excited states," Phys. Chem. Chem. Phys. 22, 3744 (2020).
- ²³ R. Sarangi, M. L. Vidal, S. Coriani, and A. I. Krylov, "On the basis set selection for calculations of core-level states: Different strategies to balance cost and accuracy," Mol. Phys. **118**, e1769872 (2020).
- ²⁴Z.-H. Loh, G. Doumy, C. Arnold, L. Kjellsson, S. H. Southworth, A. Al Haddad, Y. Kumagai, M.-F. Tu, P. J. Ho, A. M. March, R. D. Schaller, M. S. Bin Mohd Yusof, T. Debnath, M. Simon, R. Welsch, L. Inhester, K. Khalili, K. D. Nanda, A. I. Krylov, S. Moeller, G. Coslovich, J. Koralek, M. P. Minitti, W. F. Schlotter, J.-E. Rubensson, R. Santra, and L. Young, "Observation of the fastest chemical processes in the radiolysis of water," Science 367, 179 (2020).
- ²⁵L. Kjellsson, K. D. Nanda, J.-E. Rubensson, G. Doumy, S. H. Southworth, P. J. Ho, A. M. March, A. Al Haddad, Y. Kumagai, M.-F. Tu, T. Debnath, M. S. Bin Mohd Yusof, C. Arnold, W. F. Schlotter, S. Moeller, G. Coslovich, J. D. Koralek,

- M. P. Minitti, M. L. Vidal, M. Simon, R. Santra, Z.-H. Loh, S. Coriani, A. I. Krylov, and L. Young, "Resonant inelastic x-ray scattering reveals hidden local transitions of the aqueous OH radical," Phys. Rev. Lett. **124**, 236001 (2020).
- ²⁶ M. L. Vidal, M. Epshtein, V. Scutelnic, Z. Yang, T. Xue, S. R. Leone, A. I. Krylov, and S. Coriani, "The interplay of open-shell spin-coupling and Jahn-Teller distortion in benzene radical cation probed by x-ray spectroscopy," J. Phys. Chem. A 124, 9532 (2020).
- ²⁷Y. C. Park, A. Perera, and R. J. Bartlett, "Equation of motion coupled-cluster for core excitation spectra: Two complementary approaches," J. Chem. Phys. 151, 164117 (2019).
- ²⁸W. Skomorowski and A. I. Krylov, "Feshbach-Fano approach for calculation of Auger decay rates using equation-of-motion coupled-cluster wave functions: Theory and implementation," J. Chem. Phys. **154**, 084124 (2021), https://figshare.com/s/b2768383f9622e61b25e.
- ²⁹ J. V. Ortiz, "Dyson-orbital concepts for description of electrons in molecules," J. Chem. Phys. 153, 070902 (2020).
- ³⁰ A. I. Krylov, "From orbitals to observables and back," J. Chem. Phys. 153, 080901 (2020).
- ³¹ J. F. Stanton and J. Gauss, "Analytic energy derivatives for ionized states described by the equation-of-motion coupled cluster method," J. Chem. Phys. 101, 8938 (1994).
- ³²P. A. Pieniazek, S. E. Bradforth, and A. I. Krylov, "Charge localization and Jahn-Teller distortions in the benzene dimer cation," J. Chem. Phys. **129**, 074104 (2008).
- ³³ M. Musiał, A. Perera, and R. J. Bartlett, "Multireference coupled-cluster theory: The easy way," J. Chem. Phys. **134**, 114108 (2011).
- ³⁴K. W. Sattelmeyer, H. F. Schaefer III, and J. F. Stanton, "Use of 2h and 3h-p like coupled-cluster Tamm-Dancoff approaches for the equilibrium properties of ozone," Chem. Phys. Lett. **378**, 42 (2003).
- ³⁵T. Kuś and A. I. Krylov, "Using the charge stabilization technique in the double ionization potential equation-of-motion calculations with dianion references," J. Chem. Phys. **135**, 084109 (2011).
- ³⁶D. Bokhan, D. N. Trubnikov, A. Perera, and R. J. Bartlett, "Explicitly-correlated double ionization potentials and double electron attachment equation-of-motion coupled cluster methods," Chem. Phys. Lett. 692, 191 (2018).
- ³⁷ A. Perera, R. W. Molt, Jr., V. F. Lotrich, and R. J. Bartlett, "Singlet-triplet separations of di-radicals treated by the DEA/DIP-EOM-CCSD methods," in *Isaiah Shavitt*, Volume 9 of A Memorial Festschrift From Theoretical Chemistry Accounts, edited by C. J. Cramer and D. G. Truhlar (Springer, 2016), pp. 153–165.
- pp. 153–165.

 38 H. Sekino and R. J. Bartlett, "A linear response, coupled-cluster theory for excitation energy," Int. J. Quant. Chem. 26, 255 (1984).
- ³⁹H. Koch, H. J. Aa. Jensen, P. Jørgensen, and T. Helgaker, "Excitation energies from the coupled clusters singles and doubles linear response functions (CCSDLR). Applications to Be, CH⁺, CO, and H₂O," J. Chem. Phys. **93**, 3345 (1990).
- ⁴⁰ R. Krishnan, J. S. Binkley, R. Seeger, and J. A. Pople, "Self-consistent molecular orbital methods. XX. A basis set for correlated wave functions," J. Chem. Phys. 72, 650 (1980).
- ⁴¹ M. J. Frisch, J. A. Pople, and J. S. Binkley, "Self-consistent molecular orbital methods 25. Supplementary functions for Gaussian basis sets," J. Chem. Phys. **80**, 3265 (1984).
- ⁴²M. S. Szczygieł, M. Lesiuk, and R. Moszynski, "Theoretical description of the ionization processes with a discrete basis set representation of the electronic continuum," arXiv:1909.07833 (2019).
- ⁴³Y. Shao, Z. Gan, E. Epifanovsky, A. T. B. Gilbert, M. Wormit, J. Kussmann, A. W. Lange, A. Behn, J. Deng, X. Feng, D. Ghosh, M. Goldey, P. R. Horn, L. D. Jacobson, I. Kaliman, R. Z. Khaliullin, T. Kuś, A. Landau, J. Liu, E. I. Proynov, Y. M. Rhee, R. M. Richard, M. A. Rohrdanz, R. P. Steele, E. J. Sundstrom, H. L. Woodcock III, P. M. Zimmerman, D. Zuev, B. Albrecht, E. Alguire, B. Austin, G. J. O. Beran, Y. A. Bernard, E. Berquist, K. Brandhorst, K. B. Bravaya, S. T. Brown, D. Casanova, C.-M. Chang, Y. Chen, S. H. Chien, K. D. Closser, D. L. Crittenden, M. Diedenhofen, R. A. DiStasio, Jr., H. Do, A. D. Dutoi, R. G. Edgar, S. Fatehi, L. Fusti-Molnar, A. Ghysels, A. Golubeva-Zadorozhnaya, J. Gomes, M. W. D. Hanson-Heine, P. H. P. Harbach, A. W. Hauser, E. G. Hohenstein, Z. C. Holden,

- T.-C. Jagau, H. Ji, B. Kaduk, K. Khistyaev, J. Kim, J. Kim, R. A. King, P. Klunzinger, D. Kosenkov, T. Kowalczyk, C. M. Krauter, K. U. Lao, A. D. Laurent, K. V. Lawler, S. V. Levchenko, C. Y. Lin, F. Liu, E. Livshits, R. C. Lochan, A. Luenser, P. Manohar, S. F. Manzer, S.-P. Mao, N. Mardirossian, A. V. Marenich, S. A. Maurer, N. J. Mayhall, E. Neuscamman, C. M. Oana, R. Olivares-Amaya, D. P. O'Neill, J. A. Parkhill, T. M. Perrine, R. Peverati, A. Prociuk, D. R. Rehn, E. Rosta, N. J. Russ, S. M. Sharada, S. Sharma, D. W. Small, A. Sodt, T. Stein, D. Stück, Y.-C. Su, A. J. W. Thom, T. Tsuchimochi, V. Vanovschi, L. Vogt, O. Vydrov, T. Wang, M. A. Watson, J. Wenzel, A. White, C. F. Williams, J. Yang, S. Yeganeh, S. R. Yost, Z.-Q. You, I. Y. Zhang, X. Zhang, Y. Zhao, B. R. Brooks, G. K. L. Chan, D. M. Chipman, C. J. Cramer, W. A. Goddard III, M. S. Gordon, W. J. Hehre, A. Klamt, H. F. Schaefer III, M. W. Schmidt, C. D. Sherrill, D. G. Truhlar, A. Warshel, X. Xu, A. Aspuru-Guzik, R. Baer, A. T. Bell, N. A. Besley, J.-D. Chai, A. Dreuw, B. D. Dunietz, T. R. Furlani, S. R. Gwaltney, C.-P. Hsu, Y. Jung, J. Kong, D. S. Lambrecht, W. Liang, C. Ochsenfeld, V. A. Rassolov, L. V. Slipchenko, J. E. Subotnik, T. Van Voorhis, J. M. Herbert, A. I. Krylov, P. M. W. Gill, and M. Head-Gordon, "Advances in molecular quantum chemistry contained in the Q-Chem 4 program package," Mol. Phys. 113, 184 (2015).
- ⁴⁴A. I. Krylov and P. M. W. Gill, "Q-Chem: An engine for innovation," Wiley Interdiscip. Rev.: Comput. Mol. Sci. 3, 317 (2013).
- ⁴⁵S. Wolfram, *Mathematica* (Wolfram Research, Inc., 2020).
- 46 A. Albiez, M. Thoma, W. Weber, and W. Mehlhorn, " $KL_{2,3}$ ionization in neon by electron impact in the range 1.5–50 keV: Cross sections and alignment," Z. Phys. D **16**, 97 (1990).
- ⁴⁷Y. Sakai and T. Anno, "New set of rules of the Slater type on the screening constants and the effective principal quantum numbers," J. Chem. Phys. 60, 620 (1974).
- ⁴⁸ A. Müller, D. Bernhardt, A. Borovik, Jr., T. Buhr, J. Hellhund, K. Holste, A. L. D. Kilcoyne, S. Klumpp, M. Martins, S. Ricz, J. Seltmann, J. Viefhaus, and S. Schippers, "Photoionization of Ne atoms and Ne⁺ ions near the *K* edge: Precision spectroscopy and absolute cross-sections," Astrophys. J. **836**, 166 (2017).
- 49 G. Howat, T. Aberg, and O. Goscinski, "Relaxation and final-state channel mixing in the Auger effect," J. Phys. B 11, 1575 (1978).
- ⁵⁰J. Tulkki, T. Åberg, A. Mäntykenttä, and H. Aksela, "Relativistic multichannel calculation of the Ne *KLL* and Ar $L_2M_{2,3}M_{2,3}$ Auger transition rates," Phys. Rev. A **46**, 1357 (1992).
- ⁵¹ M. Leväsalmi, H. Aksela, and S. Aksela, "Satellite structure in the *KLL* spectrum of neon," Phys. Scr. **T41**, 119 (1992).
- ⁵² M. Coreno, L. Avaldi, R. Camilloni, K. C. Prince, M. De Simone, J. Karvonen, R. Colle, and S. Simonucci, "Measurement and ab initio calculation of the Ne photoabsorption spectrum in the region of the K edge," Phys. Rev. A 59, 2494 (1999).
- ⁵³S. Svensson, N. Mårtensson, E. Basilier, P. A. Malmquist, U. Gelius, and K. Siegbahn, "Lifetime broadening and CI-resonances observed in ESCA," Phys. Scr. 14, 141 (1976).
- ⁵⁴J. M. Esteva, B. Gauthe, P. Dhez, and R. C. Karnatak, "Double excitation in the *K* absorption spectrum of neon," J. Phys. B **16**, L263 (1983).
- ⁵⁵C. M. Teodorescu, R. C. Karnatak, J. M. Esteva, A. E. Afif, and J.-P. Connerade, "Unresolvable Rydberg lines in x-ray absorption spectra of free atoms," J. Phys. B 26 4019 (1993)
- ⁵⁶L. Avaldi, G. Dawber, R. Camilloni, G. C. King, M. Roper, M. R. F. Siggel, G. Stefani, M. Zitnik, A. Lisini, and P. Decleva, "Measurement of Ne 1s and 1snl satellite photoelectron spectra near threshold," Phys. Rev. A 51, 5025 (1995).
- ⁵⁷V. Carravetta, H. Ågren, and A. Cesar, "Is the core photoelectron band of neon asymmetric or not?," Chem. Phys. Lett. 180, 358 (1991).
- ⁵⁸J. C. Slater, "Atomic shielding constants," Phys. Rev. **36**, 57 (1930).
- ⁵⁹E. Clementi and D. L. Raimondi, "Atomic screening constants from SCF functions," J. Chem. Phys. 38, 2686 (1963).
- ⁶⁰M. Guerra, P. Amaro, J. P. Santos, and P. Indelicato, "Relativistic calculations of screening parameters and atomic radii of neutral atoms," At. Data Nucl. Data Tables 117-118, 439 (2017).
- ⁶¹ L. Inhester, C. F. Burmeister, G. Groenhof, and H. Grubmüller, "Auger spectrum of a water molecule after single and double core ionization," J. Chem. Phys. 136, 144304 (2012).

- ⁶²W. E. Moddeman, T. A. Carlson, M. O. Krause, B. P. Pullen, W. E. Bull, and G. K. Schweitzer, "Determination of the *K-LL* Auger spectra of N₂, O₂, CO, NO, H₂O, and CO₂," J. Chem. Phys. 55, 2317 (1971).
- ⁶³ H. Siegbahn, L. Asplund, and P. Kelfve, "The Auger electron spectrum of water vapour," Chem. Phys. Lett. 35, 330 (1975).
- ⁶⁴H. Ågren and H. Siegbahn, "Semi-internal correlation in the auger electron spectrum of H₂O," Chem. Phys. Lett. **69**, 424 (1980).
 ⁶⁵V. Carravetta and H. Ågren, "Stieltjes imaging method for molecular Auger
- ⁶⁵V. Carravetta and H. Ågren, "Stieltjes imaging method for molecular Auger transition rates: Application to the Auger spectrum of water," Phys. Rev. A 35, 1022 (1987).
- ⁶⁶ A. Cesar, H. Ågren, and V. Carravetta, "Vibronic emission from short-lived core-hole states: Theory and applications for the water molecule," Phys. Rev. A 40, 187 (1989).
- ⁶⁷G. Öhrwall, R. F. Fink, M. Tchaplyguine, L. Ojamäe, M. Lundwall, R. R. T. Marinho, A. Naves de Brito, S. L. Sorensen, M. Gisselbrecht, R. Feifel, T. Rander, A. Lindblad, J. Schulz, L. J. Sæthre, N. Mårtensson, S. Svensson, and O. Björneholm, "The electronic structure of free water clusters probed by Auger electron spectroscopy," J. Chem. Phys. 123, 054310 (2005).
- ⁶⁸Y. Hori, M. Nishida, F. H. Lim, T. Ida, and M. Mizuno, "Simulation of molecular Auger spectra using a two-electron Dyson propagator," J. Electron Spectrosc. Relat. Phenom. **207**, 60 (2016).
- ⁶⁹R. Sankari, M. Ehara, H. Nakatsuji, Y. Senba, K. Hosokawa, H. Yoshida, A. De Fanis, Y. Tamenori, S. Aksela, and K. Ueda, "Vibrationally resolved O 1s photoelectron spectrum of water," Chem. Phys. Lett. 380, 647 (2003).
 ⁷⁰A. Kivimäki, M. Neeb, B. Kempgens, H. M. Köppe, and A. M. Bradshaw, "The
- ⁷⁰A. Kivimāki, M. Neeb, B. Kempgens, H. M. Kôppe, and A. M. Bradshaw, "The C 1s Auger decay spectrum of the molecule: The effects of vibrational fine structure, double excitations and shake-up transitions," J. Phys. B 29, 2701 (1996). ⁷¹R. Spohr, T. Bergmark, N. Magnusson, L. O. Werme, C. Nordling, and K. Siegbahn, "Electron spectroscopic investigation of Auger processes in bromine substituted methanes and some hydrocarbons," Phys. Scr. 2, 31 (1970).
- ⁷²R. R. Rye, D. R. Jennison, and J. E. Houston, "Auger spectra of alkanes," J. Chem. Phys. **73**, 4867 (1980).
- ⁷³ F. P. Larkins, L. C. Tulea, and E. Z. Chelkowska, "Auger electron spectra of molecules: The first row hydrides," Aust. J. Phys. 43, 625 (1990).
- ⁷⁴L. Asplund, U. Gelius, S. Hedman, K. Helenelund, K. Siegbahn, and P. E. M. Siegbahn, "Vibrational structure and lifetime broadening in core-ionised methane," J. Phys. B 18, 1569 (1985).
- ⁷⁵P. A. Heimann, L. J. Medhurst, M. R. F. Siggel, D. A. Shirley, C. T. Chen, Y. Ma, and F. Sette, "Zero electron kinetic energy photoemission of CH₄ and CD₄ at the carbon *K* ionization threshold," Chem. Phys. Lett. **183**, 234 (1991).
- ⁷⁶H. M. Köppe, B. S. Itchkawitz, A. L. D. Kilcoyne, J. Feldhaus, B. Kempgens, A. Kivimäki, M. Neeb, and A. M. Bradshaw, "High-resolution C 1s photoelectron spectra of methane," Phys. Rev. A 53, 4120 (1996).
 ⁷⁷T. X. Carroll, N. Berrah, J. Bozek, J. Hahne, E. Kukk, L. J. Sæthre, and T. D.
- ⁷⁷T. X. Carroll, N. Berrah, J. Bozek, J. Hahne, E. Kukk, L. J. Sæthre, and T. D. Thomas, "Carbon 1s photoelectron spectrum of methane: Vibrational excitation and core-hole lifetime," Phys. Rev. A 59, 3386 (1999).
- ⁷⁸ A. Hiltunen, S. Aksela, G. Víkor, S. Ricz, Á. Kövér, and B. Sulik, "High resolution carbon and oxygen *K–LL* Auger spectra of carbon dioxide," Nucl. Instrum. Methods Phys. Res., Sect. B **154**, 267 (1999).
- ⁷⁹J. A. Kelber, D. R. Jennison, and R. R. Rye, "Analysis of the Auger spectra of CO and CO₂," J. Chem. Phys. **75**, 652 (1981).
- ⁸⁰ H. Ågren, "On the interpretation of molecular valence Auger spectra," J. Chem. Phys. 75, 1267 (1981).
- ⁸¹ J. H. D. Eland, S. Plogmaker, P. Lablanquie, F. Penent, J. Palaudoux, C. Nicolas, E. Robert, C. Miron, and R. Feifel, "Wide range double photoionisation spectra of N₂ and CO₂," Chem. Phys. Lett. **646**, 31 (2016).
- ⁸² V. Feyer, P. Bolognesi, M. Coreno, K. C. Prince, L. Avaldi, L. Storchi, and F. Tarantelli, "Effects of nuclear dynamics in the low-kinetic-energy Auger spectra of CO and CO₂," J. Chem. Phys. **123**, 224306 (2005).
- ⁸³ R. Püttner, V. Sekushin, G. Kaindl, X.-J. Liu, H. Fukuzawa, K. Ueda, T. Tanaka, M. Hoshino, and H. Tanaka, "A vibrationally resolved C 1s⁻¹ Auger spectrum of CO₂," J. Phys. B **41**, 045103 (2008).

- ⁸⁴J. Nordgren, L. Selander, L. Pettersson, C. Nordling, K. Siegbahn, and H. Ågren, "Core state vibrational excitations and symmetry breaking in the CK and OK emission spectra of CO₂," J. Chem. Phys. **76**, 3928 (1982).
- ⁸⁵ M. Neeb, B. Kempgens, A. Kivimäki, H. M. Köppe, K. Maier, U. Hergenhahn, M. N. Piancastelli, A. Rüdel, and A. M. Bradshaw, "Vibrational fine structure on the core level photoelectron lines of small polyatomic molecules," J. Electron Spectrosc. Relat. Phenom. 88-91, 19 (1998).
- ⁸⁶T. X. Carroll, J. Hahne, T. D. Thomas, L. J. Sæthre, N. Berrah, J. Bozek, and E. Kukk, "Carbon 1 s core-hole lifetime in CO₂," Phys. Rev. A 61, 042503 (2000).
- ⁸⁷W. Persson, "The spectrum of singly ionized neon, Ne II," Phys. Scr. 3, 133 (1971).
- ⁸⁸ A. Kivimäki, S. Heinäsmäki, M. Jurvansuu, S. Alitalo, E. Nõmmiste, H. Aksela, and S. Aksela, "Auger decay at the $1s^{-1}$ np (n=3-5) resonances of Ne," J. Electron Spectrosc. Relat. Phenom. **114-116**, 49 (2001).
- 89 G. Turri, G. Battera, L. Avaldi, R. Camilloni, M. Coreno, A. Ruocco, R. Colle, S. Simonucci, and G. Stefani, "Correlation effects in Auger cascade studied by angle resolved coincidence electron spectroscopy: The $1s \rightarrow 3p$ excitation in neon," J. Electron Spectrosc. Relat. Phenom. **114-116**, 199 (2001).
- ⁹⁰Y. Tamenori and I. H. Suzuki, "Multiplet exchange Auger transitions following resonant Auger decays in Ne 1s photoexcitation," J. Phys. B 47, 145001 (2014).
- ⁹¹ S. Stock, R. Beerwerth, and S. Fritzsche, "Auger cascades in resonantly excited neon," Phys. Rev. A 95, 053407 (2017).
- ⁹²H. Aksela, S. Aksela, J. Tulkki, T. Åberg, G. M. Bancroft, and K. H. Tan, "Auger emission from the resonantly excited $1s^12s^22p^63p$ state of Ne," Phys. Rev. A **39**, 3401 (1989).
- ⁹³G. Grell, O. Kühn, and S. I. Bokarev, "Multireference quantum chemistry protocol for simulating autoionization spectra: Test of ionization continuum models for the neon atom," Phys. Rev. A 100, 042512 (2019).
- ⁹⁴M. Schmidbauer, A. L. D. Kilcoyne, H.-M. Köppe, J. Feldhaus, and A. M. Bradshaw, "Shape resonances and multielectron effects in the core-level photoionization of CO₂," Phys. Rev. A **52**, 2095 (1995).
- ⁹⁵T. Porwol, G. Illing, H.-J. Freund, H. Kuhlenbeck, M. Neumann, S. Bernstorff, W. Braun, W. von Niessen, and C.-M. Liegener, "Autoionization versus photoionization of molecular adsorbates: CO₂ physisorbed on Ni(110)," Phys. Rev. B **41**, 10510 (1990).
- 96 T. X. Carroll and T. D. Thomas, "Deexcitation electron spectroscopy of core-excited CO₂: Comparison of experiment with theory," J. Chem. Phys. **94**, 11 (1991).
- ⁹⁷P. Morin, M. Simon, C. Miron, N. Leclercq, E. Kukk, J. D. Bozek, and N. Berrah, "Role of bending in the dissociation of selective resonant inner-shell excitation as observed in CO₂," Phys. Rev. A **61**, 050701 (2000).
- ⁹⁸E. Kukk, J. D. Bozek, and N. Berrah, "Photoexcitation and Auger decay of the Renner-Teller split C 1s $\rightarrow \pi_u^*$ state in CO₂," Phys. Rev. A **62**, 032708 (2000).
- 99 E. Antonsson, M. Patanen, C. Nicolas, S. Benkoula, J. J. Neville, V. L. Sukhorukov, J. D. Bozek, P. V. Demekhin, and C. Miron, "Dynamics of the C $1s \to \pi^*$ excitation and decay in CO $_2$ probed by vibrationally and angularly resolved Auger spectroscopy," Phys. Rev. A 92, 042506 (2015).
- ¹⁰⁰F. Tarantelli, A. Sgamellotti, and L. S. Cederbaum, "The calculation of molecular Auger spectra," J. Electron Spectrosc. Relat. Phenom. 68, 297 (1994).
- ¹⁰¹ T. R. Walsh, T. E. Meehan, and F. P. Larkins, "Prediction of molecular Auger rates using a statistical model," J. Phys. B 27, 2211 (1994).
- ¹⁰²D. A. Matthews and J. F. Stanton, "A new approach to approximate equation-of-motion coupled cluster with triple excitations," J. Chem. Phys. **145**, 124102 (2016).
- ¹⁰³T.-C. Jagau, "Non-iterative triple excitations in equation-of-motion coupledcluster theory for electron attachment with applications to bound and temporary anions," J. Chem. Phys. **148**, 024104 (2018).